JACS
JOURNAL OF THE AMERICAN CHEMICAL SOCIETY

pubs.acs.org/JACS

Perspective

Photocorrosion at Irradiated Perovskite/Electrolyte Interfaces

Gergely F. Samu* and Csaba Janáky*

Cite This: J. Am. Chem. Soc. 2020, 142, 21595−21614

Read Online

ACCESS | Metrics & More | Article Recommendations | Supporting Information

ABSTRACT: Metal−halide perovskites transformed optoelectronics research and development during the past decade. They have also gained a foothold in photocatalytic and photoelectrochemical processes recently, but their sensitivity to the most commonly applied solvents and electrolytes together with their susceptibility to photocorrosion hinders such applications. Understanding the elementary steps of photocorrosion of these materials can aid the endeavor of realizing stable devices. In this Perspective, we discuss both thermodynamic and kinetic aspects of photocorrosion processes occurring at the interface of perovskite photocatalysts and photoelectrodes with different electrolytes. We show how combined in situ and operando electrochemical techniques can reveal the underlying mechanisms. Finally, we also discuss emerging strategies to mitigate photocorrosion (such as surface protection, materials and electrolyte engineering, etc.).

1. INTRODUCTION

Photovoltaic (PV), photocatalytic (PC), and photoelectrochemical (PEC) systems offer the promise to efficiently convert solar energy either directly to electricity or to industrially relevant chemicals and fuels.[1] The active component is a semiconductor (SC) that can generate free charge carriers under illumination with higher energy than the bandgap ($h\nu \geq E_{BG}$). The major differentiator between PV and PC/PEC applications is the type of interfaces employed to extract and utilize these charge carriers. In PC/PEC devices, a SC/liquid interface is present that adds more functionality (and complexity) compared to the solid/solid interfaces in PV technologies. Even though the pioneering studies on illuminated SC/liquid interfaces date back to the 1970s, an industrially relevant photocatalyst/photoelectrode still remains elusive (apart from the use of TiO_2-coated self-cleaning surfaces).[2]

Metal-halide perovskites (referred to as perovskites) possess optoelectronic properties that makes them ideal in solar energy harvesting, such as large extinction coefficient,[3,4] large carrier diffusion length and lifetime,[5,6] tunable bandgap,[7,8] and mild synthesis conditions.[9] Perovskite PVs have already reached a certified efficiency of 25.5%, which can be boosted to 29.1% when applied in tandem with Si.[10] This performance, however, has not been translated to their photocatalyst/photoelectrode counterparts.[11] Unfortunately, perovskites are extremely sensitive to most environmental factors (e.g., oxygen, moisture, heat, UV light, and especially the combination of these),[12] and this instability still inhibits and complicates their practical use (even in the field of PVs). Degradation of perovskites is generally considered to be a surface- or interface-initiated process that propagates toward the bulk material.[13,14] So far, the composition and morphology of the perovskite layer (grain boundaries),[15] choice of device constituents (charge extraction, electrode, and encapsulation layers)[16] and the passivation of various interfacial defects were scrutinized in this regard.[17] Charge extraction layer/perovskite interfaces also influence the corrosion pathways.[14,18] UV light activated surface trap states of TiO_2,[19] the surface hydroxyl groups of ZnO,[20] or the interaction with the dopants from the organic hole-extraction layers are all relevant examples.[21] The effect of these factors on the stability and performance of PC/PEC systems is yet to be understood, not even mentioning the role of liquid electrolyte present.

Decomposition pathways of perovskites are regarded as purely chemical in nature, involving at least one external reactant species (such as H_2O or O_2).[18] Light can further accelerate the decomposition process (by photogenerated charge carriers) or even open additional degradation pathways (that involve redox reactions).[22,23] Furthermore, under operating conditions, the presence of electric field and the accumulation of charge carriers at different interfaces cannot be neglected.[14,24,25] Notably, significant ion traffic was observed even in the case of solid/solid interfaces. While the perovskite constituents often migrate deep into the charge extraction layers, reactive degradation products (such as I_2) can corrode the back contacts, leading to device failure.[26,27] Simultaneously, the organic cations (such as $CH_3NH_3^+$ (MA^+)) can be electrochemically reduced forming volatile products.[25] In the case of PC/PEC devices, a further complication arises because of mass transfer through the SC/liquid junction. Specifically, migrating ions can leave the perovskite lattice and dissolve in the solution, making the light-driven processes irreversible.[28−31] Combined electrochemical techniques are powerful tools to study these corrosion events in a fast and reliable manner. Once the elementary processes are uncovered, effective corrosion-mitigation strategies can be developed.

While photocorrosion studies on perovskites are still absent, much can be learned from precedent work on other SCs.[32]

Received: September 28, 2020
Published: December 18, 2020

https://dx.doi.org/10.1021/jacs.0c10348
J. Am. Chem. Soc. 2020, 142, 21595−21614

During corrosion, either complete self-decomposition or the formation of active or inactive surface layers can occur. We can approach the underlying processes from a thermodynamics perspective (i.e., whether it can happen or not); however, the convoluted reaction kinetics (i.e., multiple steps, chemical transitions) must also be considered. Corrosion events can be divided into four categories: (i) chemical, where no net charge transfer occurs at the interface; (ii) electrochemical, where the selectively injected charge carriers induce corrosion; (iii) photoelectrochemical, where the photoexcited minority carriers are predominantly responsible for the corrosion; (iv) photochemical, where both the minority and majority charge carriers can induce chemical changes. In the case of photochemical corrosion there is no external driving force that removes the majority carriers (as opposed to photoelectrochemical corrosion). Therefore, a larger fraction of majority carriers can reach the photocatalyst surface and can induce corrosion processes.

In this Perspective, we discuss the last three corrosion processes from the above list, highlighting the peculiar features of perovskites. First, we present some general thermodynamic and kinetics aspects of photocorrosion. Selected examples of corrosion processes of perovskite photocatalysts and photoelectrodes form the main body of the article, where photo(electro)catalytic and photo(electro)synthetic examples are both scrutinized. This is followed by a compilation of in situ/operando methods, which provide mechanistic insights with spatial and temporal resolution. Finally, we discuss possible mitigation strategies, which also outline future research and development avenues.

2. GENERAL CONSIDERATIONS

2.1. Thermodynamics of Photocorrosion. During electrochemical charge carrier injection, the effect of one type of charge carrier (i.e., electron or hole) can be probed selectively. In stark contrast, under light illumination, both electrons and holes are generated in SCs simultaneously, and both can induce (photo)corrosion. By comparing the electrochemical potential of these charge carriers (conduction band (CB) position for electrons and valence band (VB) position for holes) with the redox potential of the respective decomposition reaction, the stability of the SC can be evaluated.[33−35] During anodic (oxidative) corrosion reactions, the potential of holes should be more negative (on the vacuum scale), than the decomposition potential of the SC (eq 1). Meanwhile, for cathodic (reductive) corrosion reactions, the potential of electrons should be less negative than the decomposition potential (eq 2). Figure 1 illustrates the four different scenarios: (A) stable against overall photocorrosion, (B) susceptible to cathodic corrosion, (C) susceptible to anodic corrosion, (D) sensitive toward both cathodic and anodic corrosions. Based on this classification, the prototypical $MAPbI_3$ likely falls into the B category, where the direct decomposition proceeds through cathodic photocorrosion.[36]

$$AB + zh^+ \rightarrow A_{solv}^{z+} + B \quad (E_h \leq {}_pE_{decomp}) \tag{1}$$

$$AB + ze^- \rightarrow A + B_{solv}^{z-} \quad (E_e \geq {}_nE_{decomp}) \tag{2}$$

The band diagram of a p-type SC electrode (category B, common case for perovskites) is shown in Figure 2. Under equilibrium conditions (without illumination), the Fermi level (E_F) of the SC and the redox potential of the electrolyte (E_{redox}) equalizes (Figure 2A). Under illumination, the quasi-Fermi level of electrons deviates from the equilibrium value (Figure 2B). In the case of a slow redox reaction the surface concentration of electrons, and thus the quasi-Fermi levels are only slightly affected. In this situation, both the cathodic corrosion and the redox reaction can occur simultaneously. Therefore, stability can only be achieved if the corrosion kinetics is slow (scenario 1). If the redox reaction is fast, however, it can consume the surface electrons to such an extent, that the quasi-Fermi level drops below the electrochemical potential necessary to induce cathodic corrosion (scenario 2).

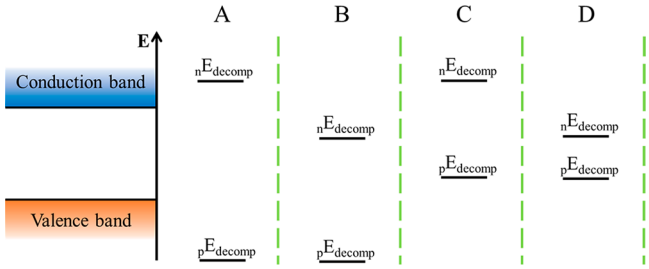

Figure 1. Photocorrosion stability of SCs based on the position of the decomposition potentials relative to the band edge energies. (A) Stable against photocorrosion, (B) stable against anodic but susceptible to cathodic corrosion, (C) stable against cathodic but sensitive to anodic corrosion, and (D) sensitive toward both cathodic and anodic corrosion. Adapted from ref 33 with permission from Elsevier, copyright 1977. ${}_nE$ and ${}_pE$ stands for negative and positive charge induced decomposition process, respectively.

In realistic situations, perovskite surfaces are not perfectly flat on the atomic scale and contain various surface structures (e.g., grain boundaries, dislocations, terraces, and valleys).[37] Such structural features are pronounced in nanostructured materials. As the coordination of the atoms occupying these surface imperfections is lower, compared to the ones situated in the bulk, they become thermodynamically more susceptible to corrosion. These sites can be the initiators of the corrosion processes, which proceed in an accelerated fashion as the surface becomes more defective in the process. It is difficult to predict the exact corrosion potential of these sites, as it requires the complete understanding of the corrosion mechanism. Furthermore, these states can also act as recombination centers, promote dark reactions, or even cause Fermi-level pinning.[35] Finally, the species present in the electrolyte can coordinate to these surface atoms weakening their back-bonds to the bulk and ultimately changing their corrosion potential.[38] At the same time, nanostructured perovskites can also offer beneficial properties that increase efficiency such as (i) short or directional charge carrier collection, (ii) tunable light distribution, (iii) quantum size effects, and (iv) increased surface area.[39,40]

2.2. Kinetics of Photocorrosion. Different kinetic models were developed to describe the mechanism of photocorrosion and to evaluate the photostability of SCs.[41] These models exclusively focus on hole-induced decomposition (anodic decomposition) and also take into account the charge carrier generation and recombination (surface or bulk) processes. As multiple participating species[42,43] and interdependent steps[44] can be involved in the overall reaction scheme, it often becomes complex. Models rely on the description of the stepwise breaking of the back-bonds of surface atoms (following charge carrier generation). In the initial step, charge carriers generated in the bulk are captured by these back-bonds. In a subsequent chemical step, a component of the electrolyte stabilizes the radical-like intermediate. The capture of a second charge carrier results in

https://dx.doi.org/10.1021/jacs.0c10348
J. Am. Chem. Soc. 2020, 142, 21595−21614

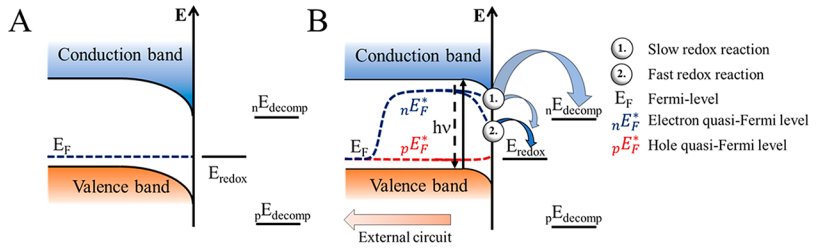

Figure 2. (A) p-type SC electrode in the dark in contact with an electrolyte with a redox active species (E_{redox}) present, showing a depletion layer with arbitrary depth. (B) p-type SC electrode under illumination and in contact with an electrolyte with a redox active species, where the redox reaction is (1) slow and (2) fast. Adapted from ref 35 with permission from Royal Society of Chemistry.

the cleavage of the back bonds of the surface atoms, resulting in decomposition. Some sophisticated models consider these intermediates to be mobile on the surface.[42,43] These elaborate models have important implications for perovskites, where light irradiation,[45−47] applied electrical bias,[48−50] or heat[51] induce halide ion migration even within the perovskite lattice. Further complications arise when solution chemistry considerations (e.g., complexation, solution phase equilibria, multiple charge carrier redox processes) are taken into account.[43,52−55] A detailed discussion of the different steps is given in the SI. Although these studies were exclusively conducted on single crystal surfaces, the profound effect of surface imperfections on the corrosion rate was realized early on.[52,56,57]

The stabilization effect of redox couples can also be included in kinetic models, as either competing reactions for surface charge carriers or reactants that regenerate the partially broken surface bonds. Generally, the stabilization efficiency of a given redox pair is light intensity dependent.[44,58,59] As the light intensity increases, the branching ratio between photocorrosion and the redox reaction shifts in favor of the decomposition process. In comparison, the stabilization efficiency of redox couples in the case of layered 2D materials was independent from the light intensity.[56] This behavior was explained by (i) the reversibility of the first charge carrier capture step and (ii) the fact that orbitals involved in driving the redox reaction, were not involved in bond formation.[34] Similar enhanced stability was found for 2D perovskites compared to their 3D counterparts.[60]

Importantly, redox couples cannot be used (unless as mediators) in solar chemical or fuel production scenarios, as their presence will also suppress the desired reaction. In these situations, the kinetics (i.e., the branching ratio) will determine the degree of suppression. Therefore, the "holy grail" would be to drive an industrially relevant redox reaction that simultaneously is able to suppress photocorrosion. The thermodynamic criteria toward this reaction (i.e., redox potential) is ultimately limited by (i) the band positions, (ii) the corrosion potentials, and (iii) the bandgap of the perovskite.[61] At this point, it is important to distinguish between photo(electro)catalytic or photo(electro)synthetic processes.[2,62] Light-driven reactions that are thermodynamically "downhill" ($\Delta G < 0$) can be termed photo(electro)catalytic, while thermodynamically "uphill" ($\Delta G < 0$) reactions are considered photo(electro)synthetic processes. In the case of photo(electro)catalytic systems, no net energy is stored in the formation of chemical bonds, the role of light is only to accelerate the otherwise sluggish reaction.

3. SPECIFICS OF PEROVSKITE PHOTOCORROSION

Perovskites are nonconventional intrinsic semiconductors. Through the introduction of cation vacancies (lead and methylammonium) p-type behavior can be achieved, while from the presence of anion vacancies (iodide), n-type behavior can be achieved.[63] These defect sites can also be formed at the charge extraction layer/perovskite interfaces during the operation of solar energy conversion devices, pointing toward the active ion conducting nature of these materials.[64] The anion in the perovskite lattice affects the activation energy of ion migration, because of the difference in the Pb−X bond strength and the vacancy density (which are the active participants in ion migration).[65] For example, halide ion migration is more pronounced in $MAPbI_3$ compared to $MAPbBr_3$. Interestingly, the migration of MA^+ is also faster as a result of the expanded lattice of $MAPbI_3$.[65] While these mobile ions in the "soft" perovskite lattice are the main reasons behind the instability, they also allow the synthesis of perovskites with defect-free bulk structure using solution phase processes.[9] Furthermore, these mobile ions are found to be the key reason for the self-healing properties of perovskites.[66] The ambipolar charge carrier transport (with charge carrier diffusion length in the micrometer range) allows efficient electron or hole extraction from the bulk. Therefore, both oxidation and reduction reactions can be driven on perovskite surfaces, especially when appropriate charge extraction interfaces are used.[67]

3.1. Corrosion of Perovskite Photocatalysts. To enable efficient PC or photosynthetic reactions, photogenerated charge carriers must be efficiently transported to catalytic sites where they must live long enough (without recombining) to be consumed in the catalytic reactions. Consequently, the long charge carrier diffusion length[5,6] and lifetime[68] coupled with the suppressed surface recombination[69] of perovskites sparked an interest in their possible PC application. Furthermore, by incorporation of different anions into the perovskite structure, the band edge position can be tailored, to activate (oxidize or reduce) different organic substrates. This allows fine-tuning of reaction mechanisms.[70,71] The stability of perovskite-based PCs has been exclusively assessed through monitoring the product output and occasionally performing postrun measurements (X-ray diffraction (XRD), energy-dispersive X-ray microanalysis (EDX), X-ray photoelectron spectroscopy (XPS)).

3.1.1. CO_2 Reduction. In PC CO_2 reduction, mild polarity solvents such as ethyl-acetate[72−78] or acetonitrile[75−77] have been used as the media to ensure the stability of the perovskites. A further advantage is that CO_2 is highly soluble in these solvents (240 mM in ethyl acetate[72] and 270 mM in acetonitrile[79]). Interestingly, small quantities of water (<0.3% v/v) was also added as a proton source and hole scavenger, without seemingly compromising the stability. The other half reaction in such PC systems is oxygen evolution from the added water.[72] This aspect is often overlooked, although both water and oxygen can compromise the stability of perovskites.

https://dx.doi.org/10.1021/jacs.0c10348
J. Am. Chem. Soc. 2020, 142, 21595−21614

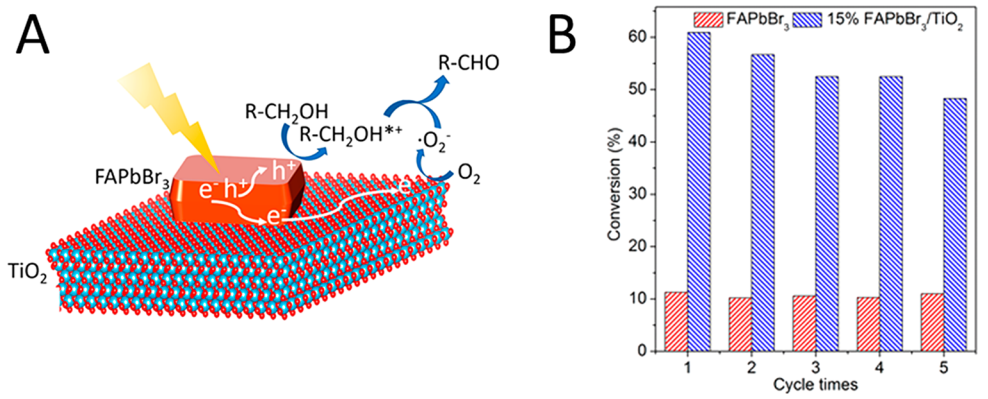

Figure 3. (A) Illustration of the mechanism of photocatalytic benzyl alcohol oxidation process over TiO_2/$FAPbBr_3$ heterojunction. (B) Recyclability of $FAPbBr_3$ and 15% $FAPbBr_3$/TiO_2 in the photocatalytic oxidation of benzyl alcohol. Reproduced with permission from ref 83. Copyright 2018 American Chemical Society.

Interestingly, the catalytic performance was relatively stable for hours.[72−78]

PC CO_2 reduction was boosted by tailoring the shape of $CsPbBr_3$ quantum dots. Through the introduction of thermodynamically less favored facets, enhanced CO and CH_4 generation was detected. After PC experiments, the facet distribution was altered, yet the catalytic output remained stable.[73] Fe(II) incorporation into $CsPbBr_3$ was also performed to control the product distribution, but most of the Fe(II) leached out from the perovskite structure during the experiment.[74] In the case of a $MAPbI_3$/Fe-based metal−organic framework (MOF), the hybrid material was more stable than the MOF itself.

A heterojunction of g-C_3N_4 and $CsPbBr_3$ nanocubes (NCs) was prepared to enhance the efficiency of charge separation. Poor recyclability was observed when the hybrid PCs were prepared via simple physical mixing.[76] When the $CsPbBr_3$ NCs were anchored on amino functionalized g-C_3N_4 through N−Br bonds, better adhesion and recyclability were achieved.[77] Similar grafting strategies were employed in the case of graphene-oxide/$CsPbBr_3$ NC[72] and MXene/$CsPbBr_3$.[78] A common feature of these studies is the slight decomposition of the ethyl acetate solvent or the ligand shell, which might form CO or CH_4 during the PC reaction.[74,76,77] While considered "insignificant" in the studies, the resulting reactive reaction products can be either participants in the CO2R reaction (like the scavengers in water splitting[80]) or detected as reaction products (e.g., CO and CH_4).[76] The contribution of these unintended side reactions shall be quantified. Furthermore, there are no experiments on the formation of liquid phase products. Currently isotope labeling studies are only carried out in a small fraction of the studies.[75−77] Such protocols for both reduction ($C^{13}O_2$)[81] and oxidation (H_2O^{18})[82] reactions are well-established. Furthermore, the PC CO_2R mechanism on perovskite NCs is still unknown, and simply observing steady product generation is not a sufficient indicator of stability.

3.1.2. PC Reactions in Organic Synthesis. A perovskite-friendly environment has to be ensured during PC organic syntheses as well. Different co-reactants and various intermediate products can all compromise the stability of the active material.[71,83] Highly nonpolar solvents have to be used (e.g., dichloromethane (DCM), hexane, toluene) that are rigorously purified from water and stabilizing agents.[70] Interestingly, upon prolonged illumination (>24 h), the decomposition of DCM can yield chloride ions, which also participate in halide ion exchange with the perovskite.[71,84] Even easier halide ion exchange occurs using the halide salt of organic reactants.[71] This can change the band edges of perovskite NCs during the PC reaction *in situ*, opening new reaction pathways.[71] Acid binding on perovskite surfaces can passivate surface defects that participate as active sites in the organic reaction.[85] The C−C bond formation between tertiary amines and aldehydes is dependent on the acidity of compounds in the reaction mixture.[71] Furthermore, smaller sized perovskite NCs had higher initial reaction rate (due to the increased surface area) but their catalytic activity diminished quickly.[71] These alterations can be monitored following the shift in the photoluminescence peak, the UV−vis absorbance onset, and the reflections on the XRD patterns.

Various perovskite-based heterojunctions (both type II and Z-scheme) were employed for the photooxidation of benzyl alcohol to benzaldehyde.[83,86,87] In the type II case, the perovskite acts as a sensitizer that injects photoexcited electrons to the CB of TiO_2 (Figure 3A).[83,86] These electrons react with molecular oxygen and form reactive superoxide radicals. The holes, remaining on the VB of perovskite, oxidize benzyl alcohol to carbocations. These react in a subsequent step with the superoxide radical, forming initially benzyl aldehyde and ultimately benzoic acid. In these PC reactions, only bromide-based (or chloride) perovskites are viable as the iodide-based counterparts are sensitive to the formed superoxide radical (eq 3). The superoxide radical can deprotonate the organic cation in the perovskite lattice and oxidize the iodide in the lattice forming iodine (which can be released into the solution phase). Importantly, this reaction also forms the basis of the light and oxygen induced degradation of perovskite solar cells.[88]

$$4CH_3NH_3PbI_3 + O_2^{\bullet-} \xrightarrow{\text{deprotonation}} 4CH_3NH_2 + 4PbI_2 + 2I_2 + 2H_2O \quad (3)$$

At its current state, all perovskite photocatalysts show poor recyclability; an example is shown in Figure 3B.[83,86] The formation of the polar reaction product (benzaldehyde) can also degrade the catalysts, as shown in the case of $FAPbBr_3$.[83] $CsPbBr_3$ recycling experiments showed fading after 4 h, while the benzyl alcohol conversion decreased from 21% to 13%. In this case, the activity decrease was attributed to the loss of catalytically active sites.[86]

A Z-scheme heterojunction was formed in the case of Bi_2WO_6/$FAPbBr_3$.[87] Upon photoexcitation and subsequent vertical charge separation, the electrons in the perovskite CB

https://dx.doi.org/10.1021/jacs.0c10348
J. Am. Chem. Soc. 2020, 142, 21595−21614

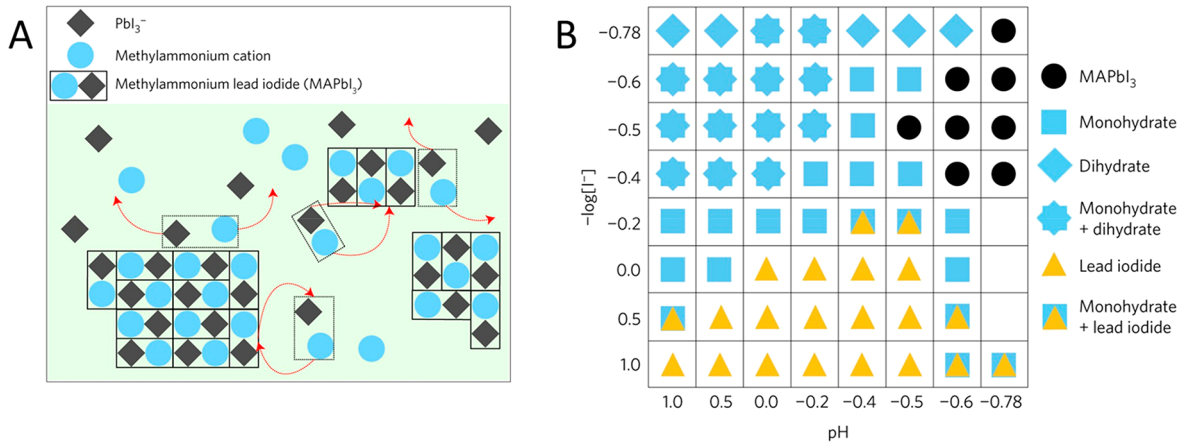

Figure 4. (A) Illustration of the dynamic equilibrium between solid $MAPbI_3$ and a saturated HI solution. (B) Effect of pH and I^- content on the chemical makeup of the precipitate formed during the equilibrium process. Reproduced from ref 95 with permission from Springer Nature.

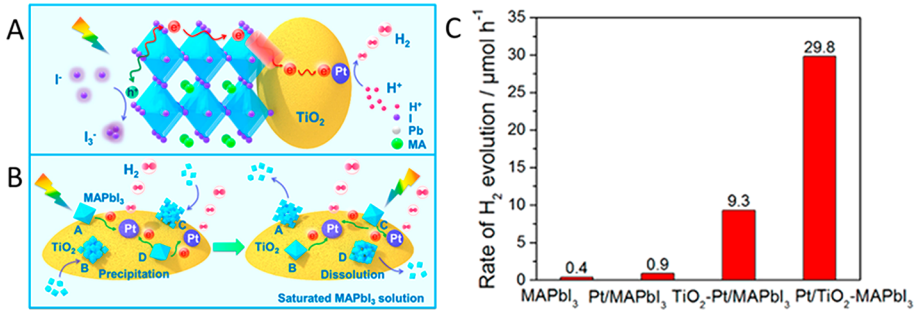

Figure 5. (A) Illustration of the flow of charge carriers in a $MAPbI_3$ + Pt/TiO_2 system during photocatalytic hydrogen evolution. (B) Proposed reaction scheme, where the TiO_2/Pt surface acts as a temporary host for the deposition of $MAPbI_3$ nanocrystals, where the charge transfer chain is established. (C) Rate of H_2 evolution of pure $MAPbI_3$, Pt decorated $MAPbI_3$, TiO_2−Pt/$MAPbI_3$ (Pt on perovskite), and Pt/TiO_2−$MAPbI_3$ (Pt on TiO_2) photocatalysts with illumination wavelengths $\lambda > 420$ nm. Reproduced with permission from ref 98. Copyright 2018 American Chemical Society.

drive CO_2 reduction to CO, while the holes in the VB of Bi_2WO_6 facilitate direct benzyl alcohol oxidation, skipping the superoxide formation step. The product evolution rates did not match the expected 1:1 stoichiometry, and superoxide formation from O_2 was also shown.[87] Furthermore, the pristine $FAPbBr_3$ showed signs of degradation, yielding CO, which calls for further studies. Perovskite PCs with varying amount of iodide vacancies were also evaluated in the PC degradation of organic compounds, and the beneficial role of iodide vacancies via the increased production of radical $O_2^{\bullet-}$ species was claimed.[89]

Surface termination can also play a role in the PC performance.[90] When $MAPbI_3$ was used for the PC conversion of 1,3-dihydroxyacetone to butyl lactate, MAI and PbI_2 terminated surfaces were synthesized. The MAI terminated surface corroded rapidly to expose Pb(II) sites, which are photocatalytically active in the reaction. As expected, the catalytic activity initially increased but soon diminished as $MAPbI_3$ was converted to PbI_2.[90] The importance of surface characteristics was further highlighted when poly(3,4-ethylenedioxythiophene) (PEDOT) was deposited on the surface of $CsPbBr_xI_{3-x}$ NCs.[91,92] When the oleic acid in the shell was replaced with methyl acetate, faster PEDOT deposition was achieved, due to the increased number of surface defects and the shorter ligand shell. The importance of the ligand shell in PC reactions was further demonstrated when the reduction of ferrocenium$^+$ (Fc^+) was only observed when the oleic acid/oleylamine was exchanged to didodecyldimethylammonium bromide (in the case, the spontaneous reduction of Fc^+ occurred).[93]

3.1.3. Hydrogen Evolution from Hydrogen Halide Solutions. When $MAPbX_3$ interacts with water, monohydrate (eq 4) and dihydrate (eq 5) phases are formed.[94] This is followed by the decomposition of the perovskite lattice, ultimately yielding insoluble PbX_2.

$$4CH_3NH_3PbI_3 + 4H_2O \rightleftharpoons 4[CH_3NH_3PbI_3 \cdot H_2O] \quad (4)$$

$$4[CH_3NH_3PbI_3 \cdot H_2O] \rightleftharpoons (CH_3NH_3)_4PbI_6 \cdot 2H_2O + 3PbI_2 + 2H_2O \quad (5)$$

These chemical corrosion steps are the basis of the moisture sensitivity of perovskite-based devices. In aqueous media, in the presence of X^-, different soluble plumbate complexes form (mainly $[PbX_3]^-$ and $[PbX_4]^{2-}$) from the water-insoluble PbX_2. In concentrated aqueous hydrogen halide solutions, these plumbate complexes form $MAPbX_3$, rather than the corrosion products (i.e., PbX_2 or the hydrated species). This dynamic equilibrium (illustrated in Figure 4A) between the corrosion (dissolution) and the reformation restructures the surface of the perovskite particles.[95] The precipitation of the perovskite occurs in a narrow pH and $[X^-]$ window (Figure 4B). The favorable band positions of perovskites (see also Figure 9) make these pseudostable systems capable of driving PC hydrogen evolution reaction (HER), which is accompanied by the respective halide oxidation reaction (a thermodynamically downhill gross

https://dx.doi.org/10.1021/jacs.0c10348
J. Am. Chem. Soc. 2020, 142, 21595−21614

Table 1. Summary of the Photoelectrochemical Performance of Unprotected Perovskite Photoelectrodes

photoelectrode	reaction	electrolyte	performance	PEC stability	light source	comment	ref
$MAPbI_3$	BQ reduction	0.1 M Bu_4NPF_6 DCM	−5.0 mA cm^{-2} (−0.4 V vs Fc/Fc^+)	50% at 22 h	100 mW cm^{-2} AM1.5G	30 μm layer	112
$MAPbI_3/PbI_2$ (2.5%)	BQ reduction	0.1 M Bu_4NPF_6 DCM	−7.0 mA cm^{-2} (−0.4 V vs Fc/Fc^+)	unknown	100 mW cm^{-2} AM1.5G	0−15% excess PbI_2	123
$(MA)_2CdCl_4$	BQ reduction	0.1 M Bu_4NPF_6 DCM	−0.35 mA cm^{-2} (−0.7 V vs Fc/Fc^+)	600 h	100 mW cm^{-2} AM1.5G	E_{BG} = 350 nm	124
$MASnBr_xI_{3-x}$	BQ reduction	0.1 M Bu_4NPF_6 DCM	−1.0 mA cm^{-2} for $MASnI_3$ (−0.7 V vs Fc/Fc^+)	50% at 40 min	100 mW cm^{-2} AM1.5G	halide composition optimization	116
$CNT/CsPbBr_xI_{3-x}NCs$	BQ reduction	0.1 M Bu_4NPF_6 DCM	−0.5 mA cm^{-2} (−0.4 V vs Fc/Fc^+)	*a*	150 mW cm^{-2} AM1.5G	Halide composition, carbon nanotube (CNT) and perovskite thickness optimization	117
$MAPbI_3$	none	0.1 M Bu_4NPF_6 DCM	0.50 μA cm^{-2} (unknown)	*a*	100 mW cm^{-2} AM1.5G	positive current flow, initial rapid current decay	102
$MAPbI_3$/CoP	none	0.1 M Bu_4NPF_6 DCM	2.00 μA cm^{-2} (unknown)	*a*	100 mW cm^{-2} AM1.5G	positive current flow, initial rapid current decay	102
$CsPbCl_xBr_{3-x}$ NCs	none	0.1 M Bu_4NPF_6 ethyl acetate	−4.4 μA cm^{-2} (unknown)	*a*	200 mW cm^{-2} AM1.5G		125
$CsPbBr_3$ NCs	none	0.1 M Bu_4NPF_6 ethyl acetate	0.1 mA cm^{-2} (unknown)	*a*	300 W Xe lamp (≥420 nm)	positive current flow	126
$CsPbBr_3$NCs/MOF (UiO-66(NH_2))	none	0.1 M Bu_4NPF_6 ethyl acetate	0.4 mA cm^{-2} (unknown)	*a*	300 W Xe lamp (≥420 nm)	positive current flow	126
$CsPbBr_3$ nanocubes	none	0.1 M Bu_4NPF_6 ethyl acetate	−0.18 mA cm^{-2}(−0.4 V vs Ag/AgCl)	*a*	150 mW cm^{-2} AM1.5G	change in PL and XRD reflection intensity	73
$CsPbBr_3$ hexapods	none	0.1 M Bu_4NPF_6 ethyl acetate	−0.10 mA cm^{-2}	*a*	150 mW cm^{-2} AM1.5G	change in PL and XRD reflection intensity	73
$CsPbBr_3$ nanocubes	none	0.1 M Bu_4NPF_6 ethyl acetate	−0.05 mA cm^{-2}	*a*	150 mW cm^{-2} AM1.5G	change in PL and XRD reflection intensity	73
$CsPbBr_3$ NCs	none	0.1 M Bu_4NPF_6 DCM	−30 μA cm^{-2} (−0.4 V vs Ag/AgCl)	*a*	150 mW cm^{-2} (≥420 nm)	in situ chemical deposition of MO_2 materials by the hydrolysis of precursors	118
$CsPbBr_3$NCs/TiO_2	none	0.1 M Bu_4NPF_6 DCM	−40 μA cm^{-2}	*a*	150 mW cm^{-2} (≥420 nm)	in situ chemical deposition of MO_2 materials by the hydrolysis of precursors	118
$CsPbBr_{3-x}Cl_x$NCs/SnO_2	none	0.1 M Bu_4NPF_6 DCM	−60 μA cm^{-2}	*a*	150 mW cm^{-2} (≥420 nm)	in situ chemical deposition of MO_2 materials by the hydrolysis of precursors	118
$CsPbBr_3$NCs/SiO_2	none	0.1 M Bu_4NPF_6 DCM	−15 μA cm^{-2}	*a*	150 mW cm^{-2} (≥420 nm)	in situ chemical deposition of MO_2 materials by the hydrolysis of precursors	118
$MAPbBr_3$	CO_2 reduction	0.1 M Bu_4NPF_6 propylene carbonate	−3 μA cm^{-2} (−0.6 V vs Ag wire)	*a*	100 mW cm^{-2} AM1.5G	unstable current response	119
GO/$MAPbBr_3$	CO_2 reduction	0.1 M Bu_4NPF_6 propylene carbonate	−5 μA cm^{-2}	*a*	100 mW cm^{-2} AM1.5G	unstable current response	119
$CsPbBr_3$ NCs	CO_2 reduction	0.1 M Bu_4NPF_6 ethyl acetate	−38.0 μA cm^{-2} (−0.4 V vs Ag/AgCl)	*a*	150 mW cm^{-2} AM1.5G	EDX reveals Fe is leached out	74
Fe:$CsPbBr_3$ NCs (25 at %)	CO_2 reduction	0.1 M Bu_4NPF_6 ethyl acetate	−120.0 μA cm^{-2}	*a*	150 mW cm^{-2} AM1.5G	EDX reveals Fe is leached out	74
g-C_3N_4/$CsPbBr_3$ NCs	CO_2 reduction	0.1 M Bu_4NPF_6 acetonitrile	−0.35 μA cm^{-2} (0 V vs Ag/AgCl)	*a*	300 W Xe lamp (≥420 nm)		77
$CsPbBr_3$NCs	CO_2 reduction	0.1 M Bu_4NPF_6 ethyl acetate	−40 μA cm^{-2} (−0.4 V vs Ag/AgCl)	*a*	150 mW cm^{-2} AM1.5G		72
GO/$CsPbBr_3$ NCs	CO_2 reduction	0.1 M Bu_4NPF_6 ethyl acetate	−50 μA cm^{-2}	*a*	150 mW cm^{-2} AM1.5G		72

https://dx.doi.org/10.1021/jacs.0c10348
J. Am. Chem. Soc. 2020, 142, 21595−21614

Table 1. continued

photoelectrode	reaction	electrolyte	performance	PEC stability	light source	comment	ref
$CsPbBr_3$ NC	CO_2 reduction	0.05 M Bu_4NPF_6 ethyl acetate	$-20\ \mu A\ cm^{-2}$ (−0.2 V vs Ag/AgCl)	*a*	150 mW cm^{-2} AM1.5G		120
$CsPbBr_3$ NC/a-TiO_2	CO_2 reduction	0.05 M Bu_4NPF_6 ethyl acetate	$-200\ \mu A\ cm^{-2}$	*a*	150 mW cm^{-2} AM1.5G		120
$CsPbBr_3/Cs_4PbBr_6$	CO_2 reduction	H_2O without added electrolyte	$-1.0\ \mu A\ cm^{-2}$ (−0.4 V vs Ag/AgCl)	*a*	100 mW cm^{-2} AM1.5G	perovskite suspension was measured	127
2%Co:$CsPbBr_3/Cs_4PbBr_6$	CO_2 reduction	H_2O without added electrolyte	$-3.0\ \mu A\ cm^{-2}$	*a*	100 mW cm^{-2} AM1.5G	perovskite suspension was measured	127
c-TiO_2/$MAPbI_3$	iodide oxidation	$MAPbI_3$-saturated aqueous HI (57%)	1.0 mA cm^{-2}(0.14 V vs Ag/AgCl)	8 h	150 mW cm^{-2} AM1.5G		106
c-TiO_2/TiO_2nanorod array/$MAPbI_3$	iodide oxidation	$MAPbI_3$-saturated aqueous HI (57%)	2.0 mA cm^{-2}	8 h	150 mW cm^{-2} AM1.5G		106
$MAPbI_3$	H_2 evolution	aqueous HI (57%) with H_3PO_2	0.75 μA (unknown)	*a*	300 W Xe lamp (≥420 nm)	positive current flow	101
$MAPbI_3/Ni_3C$	H_2 evolution	aqueous HI (57%) with H_3PO_2	1.50 μA (unknown)	*a*	300 W Xe lamp (≥420 nm)	positive current flow	101
$MAPbI_3$/black-P	H_2 evolution	$MAPbI_3$-saturated aqueous HI solution	110 μA (unknown)	*a*	300 mW Xe lamp (≥420 nm)	positive current flow	100
$MAPbBr_xI_{3-x}$	H_2 evolution	mixed aqueous HBr/HI with H_3PO_2	1.75 $\mu A\ cm^{-2}$ for $MAPbBr_{0.45}I_{2.55}$ (unknown)	*a*	300 W Xe lamp (≥420 nm)	positive current flow	97
$CsPbBr_3$ NCs	water reduction	0.1 M Na_2SO_4, water pH = 6.8	$-3\ \mu A\ cm^{-2}$ (−0.1 V vs NHE)	6 h	405 nm LED	initial current decay, with increasing dark current	121
$CsPbBr_3$NCs/TiO_2	water reduction	0.1 M Na_2SO_4, water pH = 6.8	$-5\ \mu A\ cm^{-2}$	6 h	405 nm LED	initial current decay, with increasing dark current	121
$TiO_2/CsPbBr_3$	2-mercapto-benzothiazole oxidation	0.1 M Bu_4NPF_6 DCM	0.15 mA cm^{-2} (−1.0 V vs NHE)	*a*	100 mW cm^{-2} AM1.5G	n-type behavior, slight absorbance change after PEC	128

[a]Not available.

https://dx.doi.org/10.1021/jacs.0c10348
J. Am. Chem. Soc. 2020, 142, 21595−21614

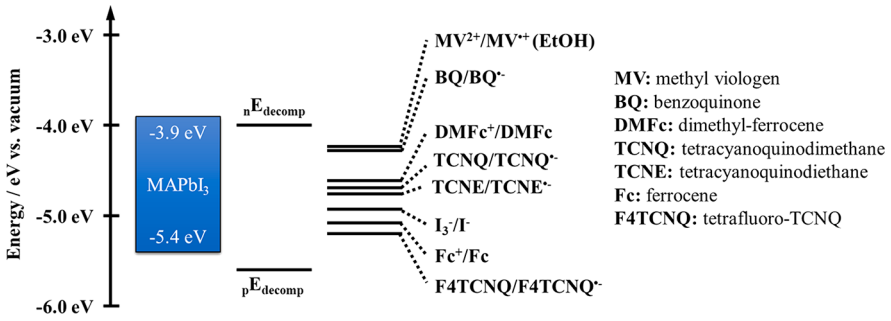

Figure 6. Band diagram of the prototypical perovskite $MAPbI_3$, together with the experimentally determined corrosion potentials. Different redox couples that have suitable redox potential to suppress corrosion processes are also shown. Adapted with permission from ref 112. Copyright 2015 American Chemical Society.

reaction). As HER progresses, X^- is simultaneously depleted from the solution and the addition of selective reducing agents (such as H_3PO_2) becomes necessary to reform the perovskite phase.

To enhance the performance (activity, selectivity, and stability) of perovskite photocatalysts in HX splitting reactions, different strategies were employed: (i) preparing mixed halide compositions,[96,97] (ii) anchoring various HER catalysts (e.g., Pt,[95,98,99] black-P,[100] rGO,[99] Ni_3C,[101] CoP,[102] Mo_2S[103]), or (iii) grafting additional hole extraction materials (e.g., PEDOT:PSS,[104] carbonized polymer dots[105]) on the perovskite surface. In the case of $TiO_2/MAPbI_3$ hybrids, a distinct difference was found in both efficiency and stability between loading the Pt on the stable TiO_2 or on the dynamically changing $MAPbI_3$ surface.[98] It was proposed that when the Pt is deposited on $MAPbI_3$ and then combined with TiO_2 in a subsequent step, the dissolution of the $MAPbI_3$ surface removes the Pt catalyst. This was not the case when the Pt catalyst was predeposited on the TiO_2 and then added to the $MAPbI_3$ containing solution (Figure 5A,B). This difference was also observed in the H_2 evolution rate (Figure 5C). Interestingly, no such behavior was observed in other cases, where Pt was directly deposited on $MAPbI_3$.[95,99−103] When one adapts this strategy to PEC applications,[106] care must be exercised as the free-standing perovskite films can be slowly dissolved into the concentrated HI solution.[98]

3.2. Corrosion of Perovskite Photoelectrodes. The existence of a photocurrent response is not sufficient to assess the stability of a given photoelectrode and might even be misleading, as photocorrosion can be a major contributor to the photocurrent.[107,108] Still, this is the widely used practice in the case of perovskite photoelectrodes. It is therefore vital to implement other characterization techniques (either ex situ or in situ) to assess their (in)stability. From the photoelectrode perspective, the initial stages of corrosion affect the surface, therefore surface-sensitive techniques (e.g., XPS) are of prime importance. As for the electrolyte solution, simple UV−vis spectroscopy can identify expelled halide species in the solution phase in micromolar concentrations.[28] More sophisticated methods such as ion chromatography or inductively coupled plasma atomic emission spectroscopy (ICP-AES) can also detect degradation products in the electrolyte.[109,110]

PEC studies carried out on unprotected perovskite photoelectrodes are summarized in Table 1. To ensure stability, most were performed in nonaqueous media (such as DCM or ethyl acetate) in the presence of different redox couples. PEC studies using benzoquinone (BQ) were superior in terms of performance and stability, as the rapid electron transfer from the perovskite to BQ (rate of 1.0×10^{10} s^{-1} from $CsPbBr_3$) can effectively suppress the cathodic photocorrosion.[111] Interestingly, other redox couples that have also suitable redox potential to suppress the cathodic corrosion (see Figure 6) have not been investigated thoroughly.[112] Similarly fast electron transfer rate from perovskites to different redox compounds was determined: 1.64×10^{10} s^{-1} to Fc^+,[93] 0.3×10^{10} s^{-1} to tetracyano-ethylene,[113] or 3.6×10^{11} s^{-1} to methylviologen (MV^{2+}).[114,115] In a similar fashion, the reduced forms of these species can accept holes from the VB of perovskites. If the binding of the redox active molecule to the surface of perovskites is strong enough and the lifetime of the charge-transfer state is long, it can participate in back-electron or hole transfer reactions.[93] These studies always focus on the charge transfer from the perovskite to the redox active molecule. The fate of the other charge carrier that is left behind is often neglected, although it can also induce corrosion. Light screening effect of these redox couple containing electrolytes has to be also addressed, either by using dilute electrolytes or through the minimization of the optical path length of the PEC cell. So far, PEC cells with $MAPbI_3$ and $BQ/BQ^{\bullet}$ redox couple performed best (-5.0 mA cm^{-2} at -0.4 V vs Fc/Fc^+ under 1 Sun).[112] In comparison, lead-free tin-containing perovskites with varying halide composition ($MASnBr_xI_{3-x}$) showed inferior performance and stability in a similar setup.[116]

Interestingly, PEC studies on perovskite photoelectrodes were only used to characterize the interaction among the constituents of the photoelectrode assemblies so far. Even during short PEC testing, some current decay was visible, which might become detrimental when translated to longer operations (Table 1). When charge-transporting layers were also employed, slightly increased current densities were observed, because of the enhanced charge carrier extraction.[72,106,117−121] Importantly, the photocurrent densities are still orders of magnitude smaller, compared to perovskite solar cells (~20 mA cm^{-2} with 1 Sun illumination (100 mW cm^{-2} AM1.5G)) for all but two entries in Table 1. This is especially striking for the CO2R and HER studies (1−100 μA cm^{-2}). Sluggish reaction kinetics or mass transport limitations alone cannot explain this behavior, as perovskite photoelectrodes with deposited catalysts also show similarly low performance. This large difference is absent in the case of other photoelectrode materials that transitioned from solar cell applications (e.g., Si and GaAs). In many studies, the exact origin of the photocurrent is unknown, as no redox couples were added to the electrolyte, and reaction products were not analyzed. In these instances, several processes can be responsible for the photocurrent such as (i) slow corrosion of the perovskite layer, (ii) decomposition of the ligand shell, or (iii) decomposition of trace amount of water or impurities in the

https://dx.doi.org/10.1021/jacs.0c10348
J. Am. Chem. Soc. 2020, 142, 21595−21614

electrolyte. In cases where CO_2 saturated electrolytes are employed, reference measurements should be carried out (under Ar-saturated conditions) as a minimum, but monitoring of the products (with isotopic labeling studies) is preferred.[81] As CO_2 often binds to the surface of the perovskite, the possibility of carbonate formation should also be addressed.[122] As noted earlier, perovskite NCs are generally stabilized with non-conductive organic molecules; therefore charge transfer through this shell is often hindered and can contribute to photocurrent losses.[114]

Perovskite-saturated hydrogen-halide electrolytes were also studied in the PEC scenario.[97,100,101,106] As the electrolyte is complex and contains different species, it is difficult to assign the photocurrent to any given process. Furthermore, the photoelectrode surface is constantly dissolving and redepositing in this media. It was also shown that perovskite layers instantly dissolved when immersed in this media.[98]

In mixed halide perovskites the bandgap monotonously decreases in the series of $Cl^- > Br^- > I^-$. For $MAPbBr_xI_{3-x}$, this translates to a bandgap variation between 1.6 eV ($x = 0$) and 2.3 eV ($x = 3$). Continuous light irradiation results in phase segregation, where iodide- and bromide-rich domains form (eq 6).[129] This process is not confined to the iodide/bromide system but was also encountered for the bromide/chloride composition.[130] Interestingly, this process is reversible, as the original mixed phase can be restored when segregated devices are stored in the dark and no solid/liquid interface is present.[28,29,45]

$$2MAPbBr_{1.5}I_{1.5} \xrightarrow{h\nu} MAPbBr_3 + MAPbI_3 \quad (6)$$

This behavior was explained by either defect[131,132] or polaron-induced[133,134] lattice strain driven migration of halide ions in the perovskite lattice. Migration can be accelerated by illumination,[45,46,49] electrical bias,[48−50] or heat.[51,135] This unique instability has a deleterious effect on the stability of perovskite PV devices;[136] however, in PC and PEC applications, it is often ignored. This is indeed surprising, because phase segregation becomes irreversible when a solid/liquid interface is also present.[28,29] Initially, the photogenerated holes trap at the iodide sites. The forming iodine/triiodide species are unstable and migrate toward the grain boundaries (phase-segregation), where they can cross the solid/liquid interface (expulsion).[28,29]

4. ELECTROCHEMICAL METHODS TO DIAGNOSE CORROSION

Electrochemistry allows selective electron or hole injection to the electrode material, which can help to uncover the elementary steps of the photocorrosion processes.[28,36,137] So far, the stability of unprotected perovskite electrodes was assessed through spectroelectrochemical experiments without external illumination.[28,36,137] The sensitivity of perovskite electrodes toward both electrons[36,137] and holes[28,36] was demonstrated. When electrons were injected to MABr-doped $FAPbI_3$ electrodes, selective dissolution was observed at the grain boundaries, followed by seemingly random intragrain pitting (Figure 7). The chemical composition of the grain boundaries were identified as a $FAPbI_3$·DMSO complex that can be easily corroded. Planes terminated in Pb^{2+} were identified as corrosion sites, and the formation of β-PbO through the oxidation of metallic Pb intermediates was proposed. This corrosion pathway was significantly suppressed by adding BQ as an electron scavenger.[137]

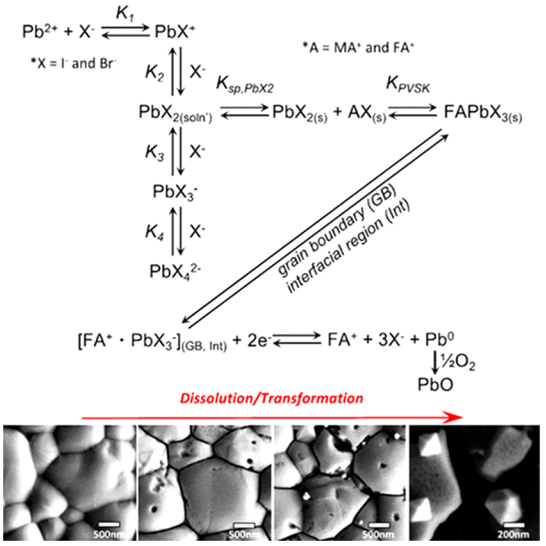

Figure 7. Summary of the reaction mechanism of formation and electrochemical corrosion of $FAPbI_3$ perovskite electrodes. SEM images showing the initial removal of the material located at the grain boundary, followed by pitting and subsequent destruction of the grains. Reproduced with permission from ref 137. Copyright 2017 American Chemical Society.

Electrochemical hole injection to $CsPbBr_3$ and $MAPbI_3$ can oxidize the halide anions in the perovskite lattice, resulting in its decomposition.[36] The situation becomes more complex in the case of *mixed* halide perovskites. Controlled hole injection to $MAPbBr_{1.5}I_{1.5}$ reveled two distinct processes.[28] The initial step of hole-trapping is not accompanied by any spectral changes (region 1 in Figure 8A). When sufficient electrochemical potential is reached to achieve hole injection into the VB of $MAPbBr_{1.5}I_{1.5}$ (region 2 in Figure 8A), however, the absorbance decreased and the bandgap changed. Hole injection gradually expelled iodide from the perovskite lattice into the solution phase, ultimately yielding pure $MAPbBr_3$ (Figure 8B), as described by eq 7.[28,29] The process possesses the hallmarks of electrochemical corrosion (Figure 8C−E). Similarly to electron injection, the corrosion also propagates from the grain boundaries.

$$4MAPbBr_{1.5}I_{1.5} + 2h^+ \rightarrow 2MAPbBr_3 + 2PbI_2 + 2MA^+ + I_2 \quad (7)$$

While detailed mechanistic studies on the photocorrosion of perovskite photoelectrodes are still lacking, different tools are available to overcome this shortcoming (see a summary in Table 2, and detailed description in the SI). Briefly, the branching ratio between corrosion and a given redox reaction can be determined by using a rotating ring disk electrode method to properly select the appropriate redox active components.[38,42,58,59,138−146] The response of a photoelectrode to periodic alteration of the incident light (studied by intensity modulated photocurrent spectroscopy, IMPS) can reveal the underlying kinetics and competition between surface recombination and the photocorrosion reaction.[147,148] Operando electrochemical techniques offer the possibility to monitor the accompanying chemical changes and evolution of corrosion intermediates during PEC reaction (either on the surface of the electrode or in the solution phase).[109,110,149−156] Furthermore, accelerated stability tests can be carried out by using ultrafast transient spectroscopic

https://dx.doi.org/10.1021/jacs.0c10348
J. Am. Chem. Soc. 2020, 142, 21595−21614

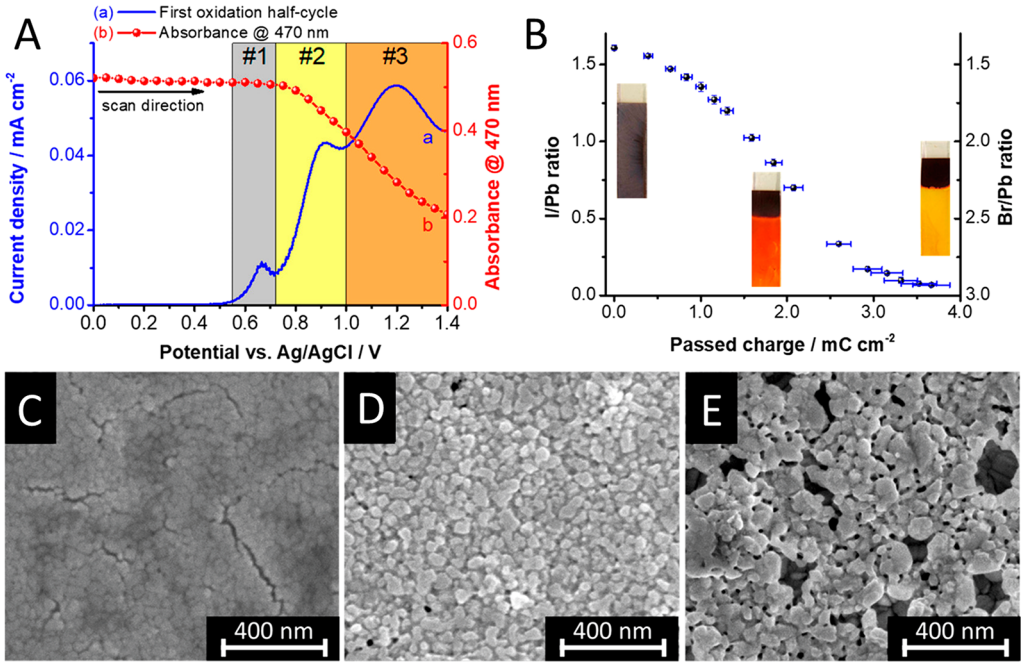

Figure 8. (A) Linear sweep voltammogram of FTO/$MAPbBr_{1.5}I_{1.5}$ film together with the absorbance change at 470 nm. Regions 1 and 2 show hole-trapping and injection to the VB, respectively. (B) Alteration of the perovskite composition as a function of passed charge during potentiostatic treatment (E = 0.9 V vs Ag/AgCl). (C–E) Top-down SEM images recorded at different stages of the hole induced corrosion. Reproduced with permission from ref 28. Copyright 2019 American Chemical Society.

Table 2. Techniques to Evaluate Photocorrosion Processes

technique	obtainable information	refs
photoelectrochemistry with illuminated rotating ring disk electrode	stabilization efficiency, reorganization energy of redox couple, active site identification of corrosion reactions	38, 42, 58, 59, 138–146
electrochemical photocapacitance spectroscopy	energy and distribution of surface states, and identification of states responsible for corrosion, efficiency of defect passivation, separation of bulk and surface states	161–164
PEC impedance spectroscopy	position of band edges, position of interband states participating in corrosion	38, 52, 146, 165–169
band edge shift measurements with corrosion current ("Tafel-plot" like representation)	stabilization efficiency, corrosion mechanism validation	38, 44, 53, 54
photocorrosion quantum efficiency measurements (monochromatic)	percentage of photocurrent attributed to corrosion (stabilization efficiency)	53, 146, 147
intensity modulated photocurrent/photovoltage spectroscopy	determination of the rate constants of distinct steps in photocorrosion, charge carrier capture cross section and activation energy of steps, mechanism evaluation	147, 148
PEC quartz crystal nanogravimetry	mass changes during PEC operation (overlayer formation, corrosion)	156, 170
in situ IR spectroelectrochemistry	identification of adsorbed species on the electrode surface, corrosion intermediate identification	155, 171
in situ Raman spectroelectrochemistry	photocorrosion product/intermediate detection	153, 154, 156
in situ UV–vis spectroelectrochemistry	material loss related to corrosion with the simultaneous evolution of dissolved species in the electrolyte; surface roughening of the electrode	28, 36, 137, 172
in situ photoluminescence spectroelectrochemistry	monitoring the formation of corrosion states, kinetics of surface corrosion state emptying and refilling	173–175
in situ PEC ICP-MS	dissolution rate during PEC operation, stoichiometry change of complex materials	109, 110
in situ PEC X-ray photoelectron spectroscopy	identification of chemical alteration of the surface/electrolyte during photocorrosion, time-evolution of corrosion products, band-alignment measurements under operating conditions	149–152
in situ UV–vis ellipsometry	change in surface layer thickness, morphology, and composition during photocorrosion	171
in situ scanning electrochemical microscopy	kinetics of photocorrosion processes	176

techniques, where the (sub-)femtosecond-pulsed irradiation can greatly accelerate the corrosion process.[157] Even subtle changes in the quality of the interfaces (trap state formation, presence of corrosion intermediates) might have an immediate impact on the charge carrier dynamics of the photoelectrode.[158,159] Careful analysis can also reveal the role of dynamically forming and recovering trap states in corrosion processes.[160]

5. DESIGN STRATEGIES TO ENHANCE STABILITY

The high degree of interchangeability of all components within the ABX_3 perovskite lattice and the vast number of different components used in related devices (e.g., charge transfer materials, surface/defect passivation agents, hydrophobic capping layers) offer different strategies to inhibit photocorrosion. Many of these are yet to be implemented in PC and PEC systems. As the first step, the relative energy positions of the components and the redox potential of the target redox

https://dx.doi.org/10.1021/jacs.0c10348
J. Am. Chem. Soc. 2020, 142, 21595–21614

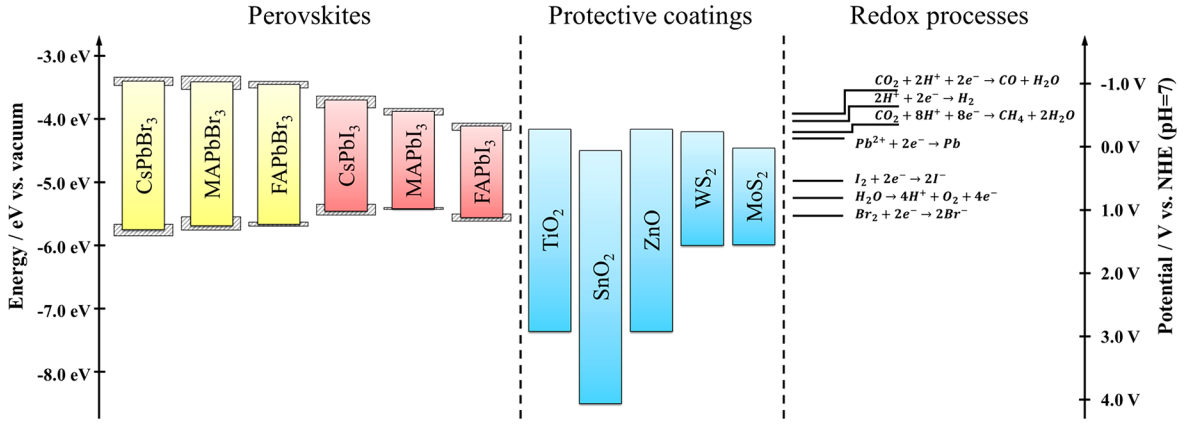

Figure 9. Band edge positions of different perovskites together with the band edge positions of some protective or catalytic coatings. The gray area around the band edges denotes the dispersion in reported values. Redox potentials of commonly encountered redox processes are also shown.

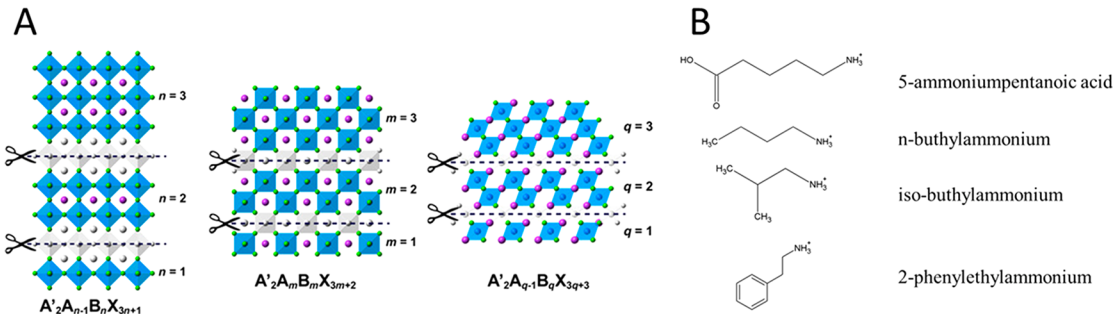

Figure 10. (A) Illustration of the different types of 2D perovskites cut through ⟨100⟩, ⟨110⟩, and ⟨111⟩ orientation. Reproduced from ref 196 with permission from Wiley-VCH. (B) Depiction of common cations used to form 2D perovskites.

reaction as well as the corrosion process have to be compared (Figure 9). To suppress corrosion, redox reactions should be introduced that are more favorable than the corrosion levels (Figure 6). As an example, through the exchange of bromide to iodide in the lattice, apart from the decrease in the optical bandgap, both band edges shift (as halogen orbitals contribute to both).[177] This decreases the pool of redox processes that can be used to stabilize iodide-containing perovskites.

The use of protective coatings is a widely employed strategy in both PC and PEC energy conversion. Possible materials combinations for driving reduction reactions are shown in Figure 9. In PC and PEC applications, however, apart from efficient charge extraction, fast transfer kinetics toward the desired substrate is also required. To overcome kinetic limitations, catalysts are often deposited on the protecting layer, which also influences the product distribution of the reactions. As shown previously, the current focus is on HER, CO2R, or oxygen evolution reaction (OER) on perovskites. Thermodynamically, these reactions are feasible, as many perovskites have proper CB and VB positions for these reactions, except for $FAPbI_3$. Notably, the reported redox potentials are generally determined in aqueous media, and deviations can occur in organic solvents. In unprotected cases, interference from the reduction of lead is expected in the HER and CO2R. In a similar manner, iodide oxidation can be problematic during OER, while bromide oxidation is less favored thermodynamically.

5.1. Compositional Engineering. The chemical instability of perovskites is mainly ascribed to the volatile organic cations (MA^+, FA^+) in the structure.[178,179] The incorporation of inorganic elements (Cs^+, Rb^+) into the structure can enhance the stability[180,181] and also suppresses phase segregation in mixed halide perovskites.[182,183] In terms of PC and PEC applications, only the mixed halide variants were studied.[89,96,97,116,117,125] With increasing bromide content in the $MAPbI_3$ lattice, the resistance to moisture was improved.[184] The susceptibility to reactive oxygen, however, remains the same.[185] The simultaneous incorporation of mixed cations, where improved stability would be expected, however, is yet to be explored. The addition of small quantities of chloride during the synthesis can suppress phase segregation.[31,186,187] It influences the perovskite film quality (morphology,[188] lattice strain,[189] grain size,[190] and crystallinity[191]) and halide defect density.[192] With decrease of the available sites that participate in phase segregation, the stability is increased in an indirect manner. Recently, triple halide perovskites were shown to be resilient toward phase segregation and operate under 100-sun intensity with less than 4% degradation for 1000 h.[186]

5.2. Crystal Facet Engineering. The various facets of perovskite crystals, which inherently have different atomic terminations, behave differently under PC or PEC operation. Properties such as (i) electronic structure, (ii) built-in electric fields, (iii) specific adsorption, (iv) reaction kinetics, (v) reaction product distribution, and (vi) stability are all affected by the exposed facets.[32,39,193] Furthermore, when multiple facets are simultaneously present, the formed heterojunction must also be considered. This can affect the charge carrier dynamics by either facilitating charge separation or enhancing charge carrier trapping.[193] The specific accumulation of charge carriers on low stability facets can accelerate corrosion. Facets with low surface energy tend to form under mild conditions, while excess energy or external stabilization (through the utilization of capping

https://dx.doi.org/10.1021/jacs.0c10348
J. Am. Chem. Soc. 2020, 142, 21595−21614

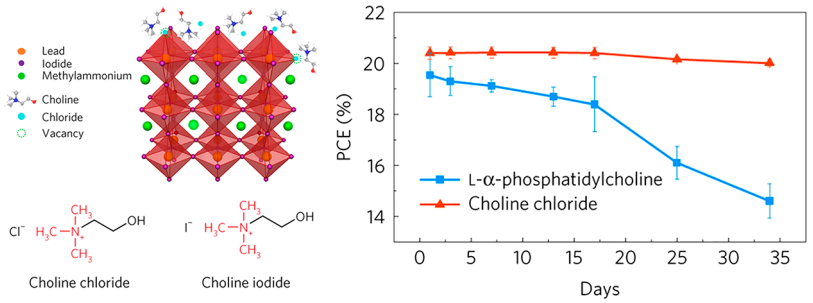

Figure 11. Depiction of surface passivation with choline chloride a quaternary ammonium halide and its beneficial effect on solar cell performance and stability. Reproduced from ref 206 with permission from Springer Nature.

agents) is necessary to form facets with high energy. Consequently, tailored exposure of selected facets can be achieved,[32,73,193] exploiting the difference in adsorption of capping agents on the various facets. Finally, when ionic species are involved in the specific adsorption, the formed electric double layer will also affect the separation of charge carriers and ultimately the kinetics of corrosion.[38] Studies on single crystal perovskites have been mainly focused on PV cells and photodetectors,[194,195] which can be later extended to PC and PEC studies.

5.3. 2D Perovskites. A unique combination of materials and crystal facet engineering is the preparation of 2D perovskite derivatives.[196] In these 2D materials, the inorganic network is disconnected along one axis, which in turn restricts charge transport to a specific plane. The perovskite lattice can be cut at crystallographic planes of ⟨100⟩, ⟨110⟩, and ⟨111⟩, resulting in the over-representation of that particular orientation (Figure 10). The ⟨100⟩ cut perovskite lattice is the most popular, as the optoelectronic properties can be varied through control over the inorganic slab thickness.[197] Two further subclasses (Ruddlesden−Popper and Dion−Jacobson perovskites) exist for the ⟨100⟩ deconstructed perovskite, based on the stacking of the inorganic layers. The large organic cations, separating the inorganic layers of the perovskite lattice, can bestow increased resistance toward humidity.[60,198,199] These organic ligands can be tailored toward specific PEC applications, providing catalytic sites for the desired reactions. Four different photoelectrode architectures can be envisioned: (i) self-standing 2D, (ii) mixed 2D/3D, (iii) 3D with 2D capping layer, and (iv) 2D passivated 3D perovskites.[196] These combinations have already attracted significant attention in the PV community, as they show superior stability but slightly inferior efficiency compared to their 3D counterparts.[60,200,201]

5.4. Surface Passivation. The ionic nature of perovskites inherently produce defects with positive (undercoordinated Pb(II) sites) or negative (undercoordinated halide ion) charge. Therefore, surface passivation is a convenient strategy to reduce the density of potentially corrosion susceptible defect states on the surface.[202] Different electron donor (Lewis-base) or acceptor (Lewis-acid) molecules can be employed to neutralize these defects. Halide containing compounds were studied as surface passivating agents, such as metal halides,[203−205] quaternary ammonium halides,[206,207] and phenylethylammonium iodide.[208,209] As an additional benefit, the efficiency of surface-passivated devices also increases, as recombination through these passivated energy levels is suppressed (Figure 11). Finally, a further physical barrier is formed against the penetration of moisture into the perovskite structure when hydrophobic ligands are employed.[210]

Corrosion processes propagate from defect sites as the chemical makeup of the intergranular layer is often susceptible to chemical attack or corrosion.[137,211] Surface passivating agents can be effectively used in the corrosion inhibition of PC and PEC systems (if their electrical conductivity is ensured). Furthermore, bifunctional molecules that possess inherent catalytic property can be also employed, therefore merging two functionalities.

5.5. Physical Coatings. Perovskite-based photoelectrodes dominantly use physically protected architectures, because with this approach the light absorber perovskite surface can be isolated from the electrolyte (buried junction concept).[212] Protection layers include metals (e.g., Ni,[213−215] Ti,[216] Field's metal[217−225]), carbon-based materials,[226,227] and atomic layer deposited TiO_2.[228] These protected photoelectrode designs employ a full (or partial) perovskite solar cell buried beneath the protective coatings. Based on the structure (n-i-p or p-i-n), both reduction and oxidation reactions can be driven on these photoelectrodes. The target reaction will dictate which charge transport layer and catalyst need to be used. Device failures are mainly caused by the penetration of electrolyte through the protective layer, due to structural imperfections. A mitigation strategy can be the incorporation of additional hydrophobic layer(s) into the structure, that can prolong the stability during PEC operation.[215,226] Further protection layers (such as polyethylenimine) were used to prevent the iodide migration to the metal contacts.[221,223−225]

Field's metal is a nontoxic eutectic alloy of bismuth (32.5%), indium (51%), and tin (16.5%), which has received considerable attention as a protective and catalytic coating. The low melting point of the alloy allows the fabrication of thick protective layers on top of the sensitive perovskite electrodes. Its use in PEC HER,[217−221,223] OER,[214,218] and CO2R[222,224,225] reactions was demonstrated. Field's metal inherently possesses catalytic activity; for example, the alloy composition had a pronounced effect on the product distribution in CO2R.[222] Furthermore, different catalytically active materials such as Pt,[217] cobalt(II)-based molecular catalysts,[224] hydrogenase enzyme,[223] or $Cu_{94}In_4$[225] can also be loaded on the surface of the photoelectrode assembly. Field's metals, however, suffer from low stability in acidic media and high cost. As a cheaper alternative, a hybrid layer of mesoporous graphite/hydrophobic graphite sheets was employed to perform OER with $CsPbBr_3$ perovskite photoanodes.[227] In this design, the mesoporous layer was responsible for charge collection, while the hydrophobic graphite sheet was used as a protective layer. An operational stability of 7−30 h (in a pH range of 2−13 in aqueous electrolyte) was demonstrated.

https://dx.doi.org/10.1021/jacs.0c10348
J. Am. Chem. Soc. 2020, 142, 21595−21614

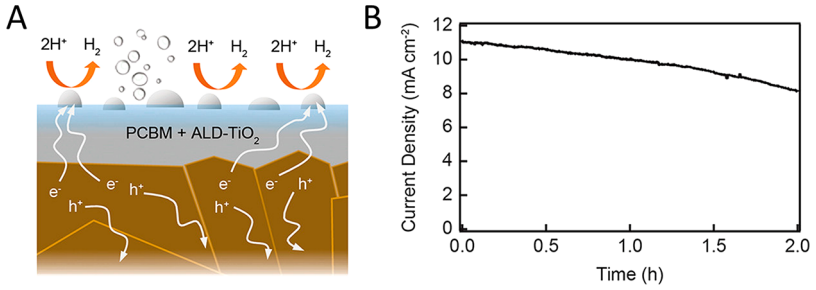

Figure 12. (A) Schematic representation of the photocathode architecture and the involved processes during photoassisted HER. (B) Stability of the photocurrent density for an ALD TiO_2 protected perovskite photocathode with a nominally 15 nm thick Pt catalyst (E = 0 V vs RHE, 0.5 Sun in 0.5 M H_2SO_4). Reproduced with permission from ref 228. Copyright 2019 American Chemical Society.

Atomic layer deposition (ALD) has been widely used to deposit different components of perovskite solar cells.[229,230] Care must be exercised when using ALD on perovskite surfaces for the deposition of (i) passivation layers, (ii) charge transfer overlayers, or (iii) encapsulation layers. The sensitivity of the perovskite surfaces toward temperature and reactants (e.g., H_2O, O_2, ozone, metal precursor), and the volatile nature of different components of perovskites (MA^+ and the I^-) have to be considered when designing the ALD protocol.[229] While ALD is considered as the state-of-the-art in depositing uniform and thin protective coatings, so far only an ALD deposited TiO_2 layer was used in the case of perovskite photoelectrodes.[228] This photocathode assembly with Pt HER catalyst (Figure 12A) was stable for 2 h in highly acidic media (pH = 0.32) under 0.5 Sun illumination (~70% activity retention) (Figure 12B). The semitransparency will enable the integration of this design into tandem PEC cells for overall solar-driven water splitting.

6. SUMMARY AND FUTURE DIRECTIONS

PC and PEC scenarios are recent additions to the potential research arenas where the optoelectronic properties of perovskites can be harnessed. Elaborating on the experience gathered from pioneering studies on photocorrosion processes and from stabilizing perovskite layers in PV devices will greatly accelerate the progress of this field. As the first step, careful characterization protocols are necessary for both PC and PEC studies (with quantitative product detection), to understand reasons and processes behind the instability. Furthermore, combined in situ electrochemical measurements will furnish mechanistic insights, with the possibility of revealing the elementary steps of corrosion. For nanoscale studies, in situ electrochemical atomic force microscopy[231−234] and PEC transmission electron microscopy will be useful to visualize morphological changes that occur on the surface of photocatalysts and photoelectrodes. Pinpointing structural weaknesses in these systems (e.g., sensitive facets, morphological features) will guide better design of stable solar energy conversion devices. In a similar fashion, coupled ultrafast techniques can shed light on how corrosion affects the charge carrier dynamics of these complex systems.[158,235] Ultrafast spectroscopic studies under electrochemical control have just been employed for perovskite electrodes recently, and further breakthroughs are expected once the pulse duration is decreased. With setups allowing few femtoseconds (or even sub-femtosecond) resolution,[236] the initial stages of charge carrier generation can be followed, providing new insights for subsequent rational materials design. While single crystal surfaces can be used to identify elementary steps in photocorrosion processes (including identification of stable and active facets), crystal facet engineering will help to translate this knowledge to nanostructured materials of practical importance.

Once the elementary steps of the photocorrosion process are uncovered, different strategies can be employed to stabilize perovskites. Compositional engineering, various surface protection approaches and the preparation of 2D perovskites are all viable options. As a particularly promising direction, bifunctional coatings can be developed, where the catalytic and protective functions are merged. Clearly, there is room for optimization, as protective coatings other than TiO_2, catalysts, and reactions (CO_2R, OER, HER) are yet to be explored (see Figure 9 for potential candidates). In this regard, emerging ALD methods will provide thin and homogeneous coatings of a rapidly broadening materials portfolio. Finally, the gathered insights on both the photocorrosion process itself and the efficiency of the mitigation strategies will provide feedback from a fresh perspective to the PV community.

Notably, corrosion processes can also be turned to our advantage. Selective removal of photoirradiated portions of samples can micropattern photoelectrodes. Furthermore, in the case of certain photoelectrodes (e.g., Cu_2O), the delicate balance between photocorrosion and the desired redox reaction is responsible for creating and maintaining the catalytically active surface (self-healing).[237] These aspects are yet to be explored in perovskite-based systems. Finally, while discussions in this Perspective focused on perovskite/electrolyte interfaces, there is a growing field of PC and PEC studies on solid/gas interfaces. Concepts borrowed from "dark" electrochemistry (such as gas-diffusion electrodes) are fueling the growth of this area, and some initial studies on perovskites are already available.[238,239]

■ ASSOCIATED CONTENT

Supporting Information

The Supporting Information is available free of charge at https://pubs.acs.org/doi/10.1021/jacs.0c10348.

Discussion on photocorrosion kinetics and summary of different techniques for studying corrosion (PDF)

■ AUTHOR INFORMATION

Corresponding Authors

Gergely F. Samu − *Department of Physical Chemistry and Materials Science, Interdisciplinary Excellence Centre, University of Szeged, Szeged H-6720, Hungary; ELI-ALPS Research Institute, Szeged H-6728, Hungary;* orcid.org/0000-0002-3239-9154; Email: samugf@chem.u-szeged.hu

https://dx.doi.org/10.1021/jacs.0c10348
J. Am. Chem. Soc. 2020, 142, 21595−21614

Csaba Janáky − *Department of Physical Chemistry and Materials Science, Interdisciplinary Excellence Centre, University of Szeged, Szeged H-6720, Hungary; ELI-ALPS Research Institute, Szeged H-6728, Hungary;* orcid.org/0000-0001-5965-5173; Email: janaky@chem.u-szeged.hu

Complete contact information is available at: https://pubs.acs.org/10.1021/jacs.0c10348

Notes

The authors declare no competing financial interest.

■ ACKNOWLEDGMENTS

The authors thank Dr. Bíborka Janáky-Bohner and Ádám Balog (both from the University of Szeged) for their constructive comments on an earlier version of the manuscript. Support from the EU's Horizon 2020 research and innovation program (Grant Agreement Nos. 716539 (ERC) and 862453) is acknowledged. The ELI-ALPS project (GINOP-2.3.6-15-2015-00001) is supported by the European Union and co-financed by the European Regional Development Fund. This project was supported by the János Bolyai Research Scholarship of the Hungarian Academy of Sciences (G.F.S.).

■ REFERENCES

(1) He, J.; Janáky, C. Recent Advances in Solar-Driven Carbon Dioxide Conversion: Expectations versus Reality. *ACS Energy Lett.* **2020**, *5*, 1996−2014.
(2) Rajeshwar, K.; Thomas, A.; Janáky, C. Photocatalytic Activity of Inorganic Semiconductor Surfaces: Myths, Hype, and Reality. *J. Phys. Chem. Lett.* **2015**, *6*, 139−147.
(3) Huang, J.; Yuan, Y.; Shao, Y.; Yan, Y. Understanding the Physical Properties of Hybrid Perovskites for Photovoltaic Applications. *Nat. Rev. Mater.* **2017**, *2*, 17042.
(4) Yin, W.-J.; Shi, T.; Yan, Y. Unique Properties of Halide Perovskites as Possible Origins of the Superior Solar Cell Performance. *Adv. Mater.* **2014**, *26*, 4653−4658.
(5) Xing, G.; Mathews, N.; Sun, S.; Lim, S. S.; Lam, Y. M.; Gratzel, M.; Mhaisalkar, S.; Sum, T. C. Long-Range Balanced Electron- and Hole-Transport Lengths in Organic-Inorganic $CH_3NH_3PbI_3$. *Science* **2013**, *342*, 344−347.
(6) Stranks, S. D.; Eperon, G. E.; Grancini, G.; Menelaou, C.; Alcocer, M. J. P.; Leijtens, T.; Herz, L. M.; Petrozza, A.; Snaith, H. J. Electron-Hole Diffusion Lengths Exceeding 1 Micrometer in an Organometal Trihalide Perovskite Absorber. *Science* **2013**, *342*, 341−344.
(7) Nedelcu, G.; Protesescu, L.; Yakunin, S.; Bodnarchuk, M. I.; Grotevent, M. J.; Kovalenko, M. V. Fast Anion-Exchange in Highly Luminescent Nanocrystals of Cesium Lead Halide Perovskites ($CsPbX_3$, X = Cl, Br, I). *Nano Lett.* **2015**, *15*, 5635−5640.
(8) Akkerman, Q. A.; D'Innocenzo, V.; Accornero, S.; Scarpellini, A.; Petrozza, A.; Prato, M.; Manna, L. Tuning the Optical Properties of Cesium Lead Halide Perovskite Nanocrystals by Anion Exchange Reactions. *J. Am. Chem. Soc.* **2015**, *137*, 10276−10281.
(9) Manser, J. S.; Saidaminov, M. I.; Christians, J. A.; Bakr, O. M.; Kamat, P. V. Making and Breaking of Lead Halide Perovskites. *Acc. Chem. Res.* **2016**, *49*, 330−338.
(10) Best Research-Cell Efficiencies https://www.nrel.gov/pv/assets/pdfs/best-research-cell-efficiencies.20200803.pdf (accessed Sep 2, 2020).
(11) Huang, H.; Pradhan, B.; Hofkens, J.; Roeffaers, M. B. J.; Steele, J. A. Solar-Driven Metal Halide Perovskite Photocatalysis: Design, Stability, and Performance. *ACS Energy Lett.* **2020**, *5*, 1107−1123.
(12) Yang, J.; Kelly, T. L. Decomposition and Cell Failure Mechanisms in Lead Halide Perovskite Solar Cells. *Inorg. Chem.* **2017**, *56*, 92−101.
(13) Deretzis, I.; Smecca, E.; Mannino, G.; La Magna, A.; Miyasaka, T.; Alberti, A. Stability and Degradation in Hybrid Perovskites: Is the Glass Half-Empty or Half-Full? *J. Phys. Chem. Lett.* **2018**, *9*, 3000−3007.
(14) Byeon, J.; Kim, J.; Kim, J.-Y.; Lee, G.; Bang, K.; Ahn, N.; Choi, M. Charge Transport Layer-Dependent Electronic Band Bending in Perovskite Solar Cells and Its Correlation to Light-Induced Device Degradation. *ACS Energy Lett.* **2020**, *5*, 2580−2589.
(15) Li, Y.; Ji, L.; Liu, R.; Zhang, C.; Mak, C. H.; Zou, X.; Shen, H.-H.; Leu, S.-Y.; Hsu, H.-Y. A Review on Morphology Engineering for Highly Efficient and Stable Hybrid Perovskite Solar Cells. *J. Mater. Chem. A* **2018**, *6*, 12842−12875.
(16) Wang, R.; Mujahid, M.; Duan, Y.; Wang, Z.; Xue, J.; Yang, Y. A Review of Perovskites Solar Cell Stability. *Adv. Funct. Mater.* **2019**, *29*, 1808843.
(17) Schulz, P.; Cahen, D.; Kahn, A. Halide Perovskites: Is It All about the Interfaces? *Chem. Rev.* **2019**, *119*, 3349−3417.
(18) Berhe, T. A.; Su, W.-N.; Chen, C.-H.; Pan, C.-J.; Cheng, J.-H.; Chen, H.-M.; Tsai, M.-C.; Chen, L.-Y.; Dubale, A. A.; Hwang, B.-J. Organometal Halide Perovskite Solar Cells: Degradation and Stability. *Energy Environ. Sci.* **2016**, *9*, 323−356.
(19) Leijtens, T.; Eperon, G. E.; Pathak, S.; Abate, A.; Lee, M. M.; Snaith, H. J. Overcoming Ultraviolet Light Instability of Sensitized TiO_2 with Meso-Superstructured Organometal Tri-Halide Perovskite Solar Cells. *Nat. Commun.* **2013**, *4*, 2885.
(20) Cheng, Y.; Yang, Q.-D.; Xiao, J.; Xue, Q.; Li, H.-W.; Guan, Z.; Yip, H.-L.; Tsang, S.-W. Decomposition of Organometal Halide Perovskite Films on Zinc Oxide Nanoparticles. *ACS Appl. Mater. Interfaces* **2015**, *7*, 19986−19993.
(21) Lee, I.; Yun, J. H.; Son, H. J.; Kim, T.-S. Accelerated Degradation Due to Weakened Adhesion from Li-TFSI Additives in Perovskite Solar Cells. *ACS Appl. Mater. Interfaces* **2017**, *9*, 7029−7035.
(22) Hong, Q.-M.; Xu, R.-P.; Jin, T.-Y.; Tang, J.-X.; Li, Y.-Q. Unraveling the Light-Induced Degradation Mechanism of $CH_3NH_3PbI_3$ Perovskite Films. *Org. Electron.* **2019**, *67*, 19−25.
(23) Akbulatov, A. F.; Luchkin, S. Y.; Frolova, L. A.; Dremova, N. N.; Gerasimov, K. L.; Zhidkov, I. S.; Anokhin, D. V.; Kurmaev, E. Z.; Stevenson, K. J.; Troshin, P. A. Probing the Intrinsic Thermal and Photochemical Stability of Hybrid and Inorganic Lead Halide Perovskites. *J. Phys. Chem. Lett.* **2017**, *8*, 1211−1218.
(24) Khenkin, M. V.; K. M., A.; Katz, E. A.; Visoly-Fisher, I. Bias-Dependent Degradation of Various Solar Cells: Lessons for Stability of Perovskite Photovoltaics. *Energy Environ. Sci.* **2019**, *12*, 550−558.
(25) Yamilova, O. R.; Danilov, A. V.; Mangrulkar, M.; Fedotov, Y. S.; Luchkin, S. Y.; Babenko, S. D.; Bredikhin, S. I.; Aldoshin, S. M.; Stevenson, K. J.; Troshin, P. A. Reduction of Methylammonium Cations as a Major Electrochemical Degradation Pathway in $MAPbI_3$ Perovskite Solar Cells. *J. Phys. Chem. Lett.* **2020**, *11*, 221−228.
(26) Kato, Y.; Ono, L. K.; Lee, M. V.; Wang, S.; Raga, S. R.; Qi, Y. Silver Iodide Formation in Methyl Ammonium Lead Iodide Perovskite Solar Cells with Silver Top Electrodes. *Adv. Mater. Interfaces* **2015**, *2*, 1500195.
(27) Guerrero, A.; You, J.; Aranda, C.; Kang, Y. S.; Garcia-Belmonte, G.; Zhou, H.; Bisquert, J.; Yang, Y. Interfacial Degradation of Planar Lead Halide Perovskite Solar Cells. *ACS Nano* **2016**, *10*, 218−224.
(28) Samu, G. F.; Balog, Á.; De Angelis, F.; Meggiolaro, D.; Kamat, P. V.; Janáky, C. Electrochemical Hole Injection Selectively Expels Iodide from Mixed Halide Perovskite Films. *J. Am. Chem. Soc.* **2019**, *141*, 10812−10820.
(29) Mathew, P. S.; Samu, G. F.; Janáky, C.; Kamat, P. V. Iodine (I) Expulsion at Photoirradiated Mixed Halide Perovskite Interface. Should I Stay or Should I Go? *ACS Energy Lett.* **2020**, *5*, 1872−1880.
(30) Kim, G. Y.; Senocrate, A.; Yang, T.-Y.; Gregori, G.; Grätzel, M.; Maier, J. Large Tunable Photoeffect on Ion Conduction in Halide Perovskites and Implications for Photodecomposition. *Nat. Mater.* **2018**, *17*, 445−449.
(31) Cho, J.; DuBose, J. T.; Mathew, P. S.; Kamat, P. V. Electrochemically Induced Iodine Migration in Mixed Halide Perovskites: Suppression through Chloride Insertion. *Chem. Commun.* **2020**, DOI: 10.1039/D0CC06217K.

(32) Toe, C. Y.; Scott, J.; Amal, R.; Ng, Y. H. Recent Advances in Suppressing the Photocorrosion of Cuprous Oxide for Photocatalytic and Photoelectrochemical Energy Conversion. *J. Photochem. Photobiol., C* **2019**, *40*, 191−211.
(33) Gerischer, H. On the Stability of Semiconductor Electrodes against Photodecomposition. *J. Electroanal. Chem. Interfacial Electrochem.* **1977**, *82*, 133−143.
(34) Gerischer, H. Electrolytic Decomposition and Photodecomposition of Compound Semiconductors in Contact with Electrolytes. *J. Vac. Sci. Technol.* **1978**, *15*, 1422−1428.
(35) Gerischer, H. Photodecomposition of Semiconductors Thermodynamics, Kinetics and Application to Solar Cells. *Faraday Discuss. Chem. Soc.* **1980**, *70*, 137−151.
(36) Samu, G. F.; Scheidt, R. A.; Kamat, P. V.; Janáky, C. Electrochemistry and Spectroelectrochemistry of Lead Halide Perovskite Films: Materials Science Aspects and Boundary Conditions. *Chem. Mater.* **2018**, *30*, 561−569.
(37) Bard, A. J.; Fan, F.-R. F.; Gioda, A. S.; Nagasubramanian, G.; White, H. S. On the Role of Surface States in Semiconductor Electrode Photoelectrochemical Cells. *Faraday Discuss. Chem. Soc.* **1980**, *70*, 19−31.
(38) Lincot, D.; Vedel, J. Adsorption of Telluride Ions on Cadmium Telluride: Consequences for Photoelectrochemical Cells. *J. Phys. Chem.* **1988**, *92*, 4103−4110.
(39) Osterloh, F. E. Inorganic Nanostructures for Photoelectrochemical and Photocatalytic Water Splitting. *Chem. Soc. Rev.* **2013**, *42*, 2294−2320.
(40) Hagfeldt, A.; Graetzel, M. Light-Induced Redox Reactions in Nanocrystalline Systems. *Chem. Rev.* **1995**, *95*, 49−68.
(41) Nandjou, F.; Haussener, S. Kinetic Competition between Water-Splitting and Photocorrosion Reactions in Photoelectrochemical Devices. *ChemSusChem* **2019**, *12*, 1984−1994.
(42) Cardon, F.; Gomes, W. P.; Vanden Kerchove, F.; Vanmaekelbergh, D.; Van Overmeire, F. On the Kinetics of Semiconductor-Electrode Stabilization. *Faraday Discuss. Chem. Soc.* **1980**, *70*, 153−164.
(43) Vanmaekelbergh, D.; Gomes, W. P. Relation between Chemical and Electrochemical Steps in the Anodic Decomposition of Group III-Group V Semiconductor Electrodes: A Comprehensive Model. *J. Phys. Chem.* **1990**, *94*, 1571−1575.
(44) Allongue, P.; Blonkowski, S.; Lincot, D. Study of Reaction Coupling and Interfacial Kinetics at Semiconductor Electrodes by Band Edge Shift Measurements. *J. Electroanal. Chem. Interfacial Electrochem.* **1991**, *300*, 261−281.
(45) Hoke, E. T.; Slotcavage, D. J.; Dohner, E. R.; Bowring, A. R.; Karunadasa, H. I.; McGehee, M. D. Reversible Photo-Induced Trap Formation in Mixed-Halide Hybrid Perovskites for Photovoltaics. *Chem. Sci.* **2015**, *6*, 613−617.
(46) Yoon, S. J.; Kuno, M.; Kamat, P. V. Shift Happens. How Halide Ion Defects Influence Photoinduced Segregation in Mixed Halide Perovskites. *ACS Energy Lett.* **2017**, *2*, 1507−1514.
(47) Brennan, M. C.; Draguta, S.; Kamat, P. V.; Kuno, M. Light-Induced Anion Phase Segregation in Mixed Halide Perovskites. *ACS Energy Lett.* **2018**, *3*, 204−213.
(48) Braly, I. L.; Stoddard, R. J.; Rajagopal, A.; Uhl, A. R.; Katahara, J. K.; Jen, A. K.-Y.; Hillhouse, H. W. Current-Induced Phase Segregation in Mixed Halide Hybrid Perovskites and Its Impact on Two-Terminal Tandem Solar Cell Design. *ACS Energy Lett.* **2017**, *2*, 1841−1847.
(49) Duong, T.; Mulmudi, H. K.; Wu, Y.; Fu, X.; Shen, H.; Peng, J.; Wu, N.; Nguyen, H. T.; Macdonald, D.; Lockrey, M.; White, T. P.; Weber, K.; Catchpole, K. Light and Electrically Induced Phase Segregation and Its Impact on the Stability of Quadruple Cation High Bandgap Perovskite Solar Cells. *ACS Appl. Mater. Interfaces* **2017**, *9*, 26859−26866.
(50) Lin, Y.; Chen, B.; Fang, Y.; Zhao, J.; Bao, C.; Yu, Z.; Deng, Y.; Rudd, P. N.; Yan, Y.; Yuan, Y.; Huang, J. Excess Charge-Carrier Induced Instability of Hybrid Perovskites. *Nat. Commun.* **2018**, *9*, 4981.
(51) Elmelund, T.; Scheidt, R. A.; Seger, B.; Kamat, P. V. Bidirectional Halide Ion Exchange in Paired Lead Halide Perovskite Films with Thermal Activation. *ACS Energy Lett.* **2019**, *4*, 1961−1969.
(52) Allongue, P.; Cachet, H. Photodissolution Kinetics of n-GaAs in 1M KOH and Calculation of the Stabilization by Se^{2-}: Effect of the Ru^{3+} Surface Treatment. *J. Electrochem. Soc.* **1984**, *131*, 2861−2868.
(53) Allongue, P.; Blonkowski, S. Corrosion of III-V Compounds; a Comparative Study of GaAs and InP Part I. Electrochemical Characterization Based on Tafel Plot Measurements. *J. Electroanal. Chem. Interfacial Electrochem.* **1991**, *316*, 57−77.
(54) Allongue, P.; Blonkowski, S. Corrosion of III-V Compounds; a Comparative Study of GaAs and InP II. Reaction Scheme and Influence of Surface Properties. *J. Electroanal. Chem. Interfacial Electrochem.* **1991**, *317*, 77−99.
(55) Benito, R. M.; Nozik, A. J. Theoretical Analysis of the Effects of Light Intensity on the Photocorrosion of Semiconductor Electrodes. *J. Phys. Chem.* **1985**, *89*, 3429−3434.
(56) Gerischer, H.; Lübke, M. Competition between Photocorrosion and Photooxidation of Redox Systems at n-Type Semiconductor Electrodes. *Berichte der Bunsengesellschaft für Phys. Chemie* **1983**, *87*, 123−128.
(57) Kautek, W.; Gerischer, H. Anisotropic Photocorrosion of N-Type MoS_2 $MoSe_2$, and WSe_2 Single Crystal Surfaces: The Role 0f Cleavage Steps, Line and Screw Dislocations. *Surf. Sci.* **1982**, *119*, 46−60.
(58) Frese, K. W.; Madou, M. J.; Morrison, S. R. Investigation of Photoelectrochemical Corrosion of Semiconductors. 1. *J. Phys. Chem.* **1980**, *84*, 3172−3178.
(59) Reineke, R.; Memming, R. Comparability of Redox Reactions at n- and p-Type Semiconductor Electrodes. 1. The Quasi-Fermi Level Concept. *J. Phys. Chem.* **1992**, *96*, 1310−1317.
(60) Tsai, H.; Nie, W.; Blancon, J.-C.; Stoumpos, C. C.; Asadpour, R.; Harutyunyan, B.; Neukirch, A. J.; Verduzco, R.; Crochet, J. J.; Tretiak, S.; Pedesseau, L.; Even, J.; Alam, M. A.; Gupta, G.; Lou, J.; Ajayan, P. M.; Bedzyk, M. J.; Kanatzidis, M. G.; Mohite, A. D. High-Efficiency Two-Dimensional Ruddlesden-Popper Perovskite Solar Cells. *Nature* **2016**, *536*, 312−316.
(61) Guo, L.-J.; Luo, J.-W.; He, T.; Wei, S.-H.; Li, S.-S. Photocorrosion-Limited Maximum Efficiency of Solar Photoelectrochemical Water Splitting. *Phys. Rev. Appl.* **2018**, *10*, 064059.
(62) Osterloh, F. E. Photocatalysis versus Photosynthesis: A Sensitivity Analysis of Devices for Solar Energy Conversion and Chemical Transformations. *ACS Energy Lett.* **2017**, *2*, 445−453.
(63) Wang, Q.; Shao, Y.; Xie, H.; Lyu, L.; Liu, X.; Gao, Y.; Huang, J. Qualifying Composition Dependent p and n Self-Doping in $CH_3NH_3PbI_3$. *Appl. Phys. Lett.* **2014**, *105*, 163508.
(64) Frolova, L. A.; Dremova, N. N.; Troshin, P. A. The Chemical Origin of the p-Type and n-Type Doping Effects in the Hybrid Methylammonium-Lead Iodide ($MAPbI_3$) Perovskite Solar Cells. *Chem. Commun.* **2015**, *51*, 14917−14920.
(65) McGovern, L.; Futscher, M. H.; Muscarella, L. A.; Ehrler, B. Understanding the Stability of $MAPbBr_3$ versus $MAPbI_3$: Suppression of Methylammonium Migration and Reduction of Halide Migration. *J. Phys. Chem. Lett.* **2020**, *11*, 7127−7132.
(66) Tian, Y.; Peter, M.; Unger, E.; Abdellah, M.; Zheng, K.; Pullerits, T.; Yartsev, A.; Sundström, V.; Scheblykin, I. G. Mechanistic Insights into Perovskite Photoluminescence Enhancement: Light Curing with Oxygen Can Boost Yield Thousandfold. *Phys. Chem. Chem. Phys.* **2015**, *17*, 24978−24987.
(67) Schanze, K. S.; Kamat, P. V.; Yang, P.; Bisquert, J. Progress in Perovskite Photocatalysis. *ACS Energy Lett.* **2020**, *5*, 2602−2604.
(68) Yang, Y.; Yang, M.; Li, Z.; Crisp, R.; Zhu, K.; Beard, M. C. Comparison of Recombination Dynamics in $CH_3NH_3PbBr_3$ and $CH_3NH_3PbI_3$ Perovskite Films: Influence of Exciton Binding Energy. *J. Phys. Chem. Lett.* **2015**, *6*, 4688−4692.
(69) Yang, Y.; Yan, Y.; Yang, M.; Choi, S.; Zhu, K.; Luther, J. M.; Beard, M. C. Low Surface Recombination Velocity in Solution-Grown $CH_3NH_3PbBr_3$ Perovskite Single Crystal. *Nat. Commun.* **2015**, *6*, 7961.

https://dx.doi.org/10.1021/jacs.0c10348
J. Am. Chem. Soc. 2020, 142, 21595−21614

(70) Zhu, X.; Lin, Y.; Sun, Y.; Beard, M. C.; Yan, Y. Lead-Halide Perovskites for Photocatalytic α-Alkylation of Aldehydes. *J. Am. Chem. Soc.* **2019**, *141*, 733−738.
(71) Zhu, X.; Lin, Y.; San Martin, J.; Sun, Y.; Zhu, D.; Yan, Y. Lead Halide Perovskites for Photocatalytic Organic Synthesis. *Nat. Commun.* **2019**, *10*, 2843.
(72) Xu, Y.-F.; Yang, M.-Z.; Chen, B.-X.; Wang, X.-D.; Chen, H.-Y.; Kuang, D.-B.; Su, C.-Y. A $CsPbBr_3$ Perovskite Quantum Dot/Graphene Oxide Composite for Photocatalytic CO_2 Reduction. *J. Am. Chem. Soc.* **2017**, *139*, 5660−5663.
(73) Shyamal, S.; Dutta, S. K.; Das, T.; Sen, S.; Chakraborty, S.; Pradhan, N. Facets and Defects in Perovskite Nanocrystals for Photocatalytic CO_2 Reduction. *J. Phys. Chem. Lett.* **2020**, *11*, 3608−3614.
(74) Shyamal, S.; Dutta, S. K.; Pradhan, N. Doping Iron in $CsPbBr_3$ Perovskite Nanocrystals for Efficient and Product Selective CO_2 Reduction. *J. Phys. Chem. Lett.* **2019**, *10*, 7965−7969.
(75) Wu, L.; Mu, Y.; Guo, X.; Zhang, W.; Zhang, Z.; Zhang, M.; Lu, T. Encapsulating Perovskite Quantum Dots in Iron-Based Metal-Organic Frameworks (MOFs) for Efficient Photocatalytic CO_2 Reduction. *Angew. Chem., Int. Ed.* **2019**, *58*, 9491−9495.
(76) You, S.; Guo, S.; Zhao, X.; Sun, M.; Sun, C.; Su, Z.; Wang, X. All-Inorganic Perovskite/Graphitic Carbon Nitride Composites for CO_2 Photoreduction into C1 Compounds under Low Concentrations of CO_2. *Dalt. Trans.* **2019**, *48*, 14115−14121.
(77) Ou, M.; Tu, W.; Yin, S.; Xing, W.; Wu, S.; Wang, H.; Wan, S.; Zhong, Q.; Xu, R. Amino-Assisted Anchoring of $CsPbBr_3$ Perovskite Quantum Dots on Porous g-C_3N_4 for Enhanced Photocatalytic CO_2 Reduction. *Angew. Chem.* **2018**, *130*, 13758−13762.
(78) Pan, A.; Ma, X.; Huang, S.; Wu, Y.; Jia, M.; Shi, Y.; Liu, Y.; Wangyang, P.; He, L.; Liu, Y. $CsPbBr_3$ Perovskite Nanocrystal Grown on MXene Nanosheets for Enhanced Photoelectric Detection and Photocatalytic CO_2 Reduction. *J. Phys. Chem. Lett.* **2019**, *10*, 6590−6597.
(79) Tomita, Y.; Teruya, S.; Koga, O.; Hori, Y. Electrochemical Reduction of Carbon Dioxide at a Platinum Electrode in Acetonitrile-Water Mixtures. *J. Electrochem. Soc.* **2000**, *147* (11), 4164.
(80) Schneider, J.; Bahnemann, D. W. Undesired Role of Sacrificial Reagents in Photocatalysis. *J. Phys. Chem. Lett.* **2013**, *4*, 3479−3483.
(81) Hursán, D.; Janáky, C. Electrochemical Reduction of Carbon Dioxide on Nitrogen-Doped Carbons: Insights from Isotopic Labeling Studies. *ACS Energy Lett.* **2018**, *3*, 722−723.
(82) Haschke, S.; Mader, M.; Schlicht, S.; Roberts, A. M.; Angeles-Boza, A. M.; Barth, J. A. C.; Bachmann, J. Direct Oxygen Isotope Effect Identifies the Rate-Determining Step of Electrocatalytic OER at an Oxidic Surface. *Nat. Commun.* **2018**, *9*, 4565.
(83) Huang, H.; Yuan, H.; Janssen, K. P. F.; Solís-Fernández, G.; Wang, Y.; Tan, C. Y. X.; Jonckheere, D.; Debroye, E.; Long, J.; Hendrix, J.; Hofkens, J.; Steele, J. A.; Roeffaers, M. B. J. Efficient and Selective Photocatalytic Oxidation of Benzylic Alcohols with Hybrid Organic-Inorganic Perovskite Materials. *ACS Energy Lett.* **2018**, *3*, 755−759.
(84) Parobek, D.; Dong, Y.; Qiao, T.; Rossi, D.; Son, D. H. Photoinduced Anion Exchange in Cesium Lead Halide Perovskite Nanocrystals. *J. Am. Chem. Soc.* **2017**, *139*, 4358−4361.
(85) Bonabi Naghadeh, S.; Luo, B.; Abdelmageed, G.; Pu, Y.-C.; Zhang, C.; Zhang, J. Z. Photophysical Properties and Improved Stability of Organic-Inorganic Perovskite by Surface Passivation. *J. Phys. Chem. C* **2018**, *122*, 15799−15818.
(86) Schünemann, S.; van Gastel, M.; Tüysüz, H. A $CsPbBr_3/TiO_2$ Composite for Visible-Light-Driven Photocatalytic Benzyl Alcohol Oxidation. *ChemSusChem* **2018**, *11*, 2057−2061.
(87) Huang, H.; Zhao, J.; Du, Y.; Zhou, C.; Zhang, M.; Wang, Z.; Weng, Y.; Long, J.; Hofkens, J.; Steele, J. A.; Roeffaers, M. B. J. Direct Z-Scheme Heterojunction of Semicoherent $FAPbBr_3/Bi_2WO_6$ Interface for Photoredox Reaction with Large Driving Force. *ACS Nano* **2020**, DOI: 10.1021/acsnano.0c03146.
(88) Aristidou, N.; Sanchez-Molina, I.; Chotchuangchutchaval, T.; Brown, M.; Martinez, L.; Rath, T.; Haque, S. A. The Role of Oxygen in the Degradation of Methylammonium Lead Trihalide Perovskite Photoactive Layers. *Angew. Chem., Int. Ed.* **2015**, *54*, 8208−8212.
(89) Gualdrón-Reyes, A. F.; Rodríguez-Pereira, J.; Amado-González, E.; Rueda-P, J.; Ospina, R.; Masi, S.; Yoon, S. J.; Tirado, J.; Jaramillo, F.; Agouram, S.; Muñoz-Sanjosé, V.; Giménez, S.; Mora-Seró, I. Unravelling the Photocatalytic Behavior of All-Inorganic Mixed Halide Perovskites: The Role of Surface Chemical States. *ACS Appl. Mater. Interfaces* **2020**, *12*, 914−924.
(90) Dong, Y.; Li, K.; Luo, W.; Zhu, C.; Guan, H.; Wang, H.; Wang, L.; Deng, K.; Zhou, H.; Xie, H.; Bai, Y.; Li, Y.; Chen, Q. The Role of Surface Termination in Halide Perovskites for Efficient Photocatalytic Synthesis. *Angew. Chem.* **2020**, *132*, 13031−13037.
(91) Chen, K.; Deng, X.; Dodekatos, G.; Tüysüz, H. Photocatalytic Polymerization of 3,4-Ethylenedioxythiophene over Cesium Lead Iodide Perovskite Quantum Dots. *J. Am. Chem. Soc.* **2017**, *139*, 12267−12273.
(92) Li, Y.; Shu, Q.; Du, Q.; Dai, Y.; Zhao, S.; Zhang, J.; Li, L.; Chen, K. Surface Modification for Improving the Photocatalytic Polymerization of 3,4-Ethylenedioxythiophene over Inorganic Lead Halide Perovskite Quantum Dots. *ACS Appl. Mater. Interfaces* **2020**, *12*, 451−460.
(93) DuBose, J. T.; Kamat, P. V. Probing Perovskite Photocatalysis. Interfacial Electron Transfer between $CsPbBr_3$ and Ferrocene Redox Couple. *J. Phys. Chem. Lett.* **2019**, *10*, 6074−6080.
(94) Christians, J. A.; Miranda Herrera, P. A.; Kamat, P. V. Transformation of the Excited State and Photovoltaic Efficiency of $CH_3NH_3PbI_3$ Perovskite upon Controlled Exposure to Humidified Air. *J. Am. Chem. Soc.* **2015**, *137*, 1530−1538.
(95) Park, S.; Chang, W. J.; Lee, C. W.; Park, S.; Ahn, H.-Y.; Nam, K. T. Photocatalytic Hydrogen Generation from Hydriodic Acid Using Methylammonium Lead Iodide in Dynamic Equilibrium with Aqueous Solution. *Nat. Energy* **2017**, *2*, 16185.
(96) Wu, Y.; Wang, P.; Guan, Z.; Liu, J.; Wang, Z.; Zheng, Z.; Jin, S.; Dai, Y.; Whangbo, M.-H.; Huang, B. Enhancing the Photocatalytic Hydrogen Evolution Activity of Mixed-Halide Perovskite $CH_3NH_3PbBr_{3-x}I_x$ Achieved by Bandgap Funneling of Charge Carriers. *ACS Catal.* **2018**, *8*, 10349−10357.
(97) Zhao, Z.; Wu, J.; Zheng, Y.-Z.; Li, N.; Li, X.; Ye, Z.; Lu, S.; Tao, X.; Chen, C. Stable Hybrid Perovskite $MAPb(I_{1-x}Br_x)_3$ for Photocatalytic Hydrogen Evolution. *Appl. Catal., B* **2019**, *253*, 41−48.
(98) Wang, X.; Wang, H.; Zhang, H.; Yu, W.; Wang, X.; Zhao, Y.; Zong, X.; Li, C. Dynamic Interaction between Methylammonium Lead Iodide and TiO2 Nanocrystals Leads to Enhanced Photocatalytic H_2 Evolution from HI Splitting. *ACS Energy Lett.* **2018**, *3*, 1159−1164.
(99) Wu, Y.; Wang, P.; Zhu, X.; Zhang, Q.; Wang, Z.; Liu, Y.; Zou, G.; Dai, Y.; Whangbo, M.-H.; Huang, B. Composite of $CH_3NH_3PbI_3$ with Reduced Graphene Oxide as a Highly Efficient and Stable Visible-Light Photocatalyst for Hydrogen Evolution in Aqueous HI Solution. *Adv. Mater.* **2018**, *30*, 1704342.
(100) Li, R.; Li, X.; Wu, J.; Lv, X.; Zheng, Y.-Z.; Zhao, Z.; Ding, X.; Tao, X.; Chen, J.-F. Few-Layer Black Phosphorus-on-$MAPbI_3$ for Superb Visible-Light Photocatalytic Hydrogen Evolution from HI Splitting. *Appl. Catal., B* **2019**, *259*, 118075.
(101) Zhao, Z.; Wu, J.; Zheng, Y.-Z.; Li, N.; Li, X.; Tao, X. Ni_3C-Decorated $MAPbI_3$ as Visible-Light Photocatalyst for H_2 Evolution from HI Splitting. *ACS Catal.* **2019**, *9*, 8144−8152.
(102) Cai, C.; Teng, Y.; Wu, J.; Li, J.; Chen, H.; Chen, J.; Kuang, D. In Situ Photosynthesis of an $MAPbI_3$/CoP Hybrid Heterojunction for Efficient Photocatalytic Hydrogen Evolution. *Adv. Funct. Mater.* **2020**, *30*, 2001478.
(103) Wang, F.; Liu, X.; Zhang, Z.; Min, S. A Noble-Metal-Free MoS_2 Nanosheet-Coupled $MAPbI_3$ Photocatalyst for Efficient and Stable Visible-Light-Driven Hydrogen Evolution. *Chem. Commun.* **2020**, *56*, 3281−3284.
(104) Wang, H.; Wang, X.; Chen, R.; Zhang, H.; Wang, X.; Wang, J.; Zhang, J.; Mu, L.; Wu, K.; Fan, F.; Zong, X.; Li, C. Promoting Photocatalytic H_2 Evolution on Organic-Inorganic Hybrid Perovskite Nanocrystals by Simultaneous Dual-Charge Transportation Modulation. *ACS Energy Lett.* **2019**, *4*, 40−47.

(105) Zhao, Y.; Zeng, Q.; Yu, Y.; Feng, T.; Zhao, Y.; Wang, Z.; Li, Y.; Liu, C.; Liu, J.; Wei, H.; Zhu, S.; Kang, Z.; Zhang, H.; Yang, B. Enhanced Charge Separation and Photocatalytic Hydrogen Evolution in Carbonized-Polymer-Dot-Coupled Lead Halide Perovskites. *Mater. Horiz.* **2020**, *7*, 2719−2725.
(106) Luo, J.; Yang, H.; Liu, Z.; Li, F.; Liu, S.; Ma, J.; Liu, B. Organic-Inorganic Hybrid Perovskite - TiO_2 Nanorod Arrays for Efficient and Stable Photoelectrochemical Hydrogen Evolution from HI Splitting. *Mater. Today Chem.* **2019**, *12*, 1−6.
(107) Kampmann, J.; Betzler, S.; Hajiyani, H.; Häringer, S.; Beetz, M.; Harzer, T.; Kraus, J.; Lotsch, B. V.; Scheu, C.; Pentcheva, R.; Fattakhova-Rohlfing, D.; Bein, T. How Photocorrosion Can Trick You: A Detailed Study on Low-Bandgap Li Doped CuO Photocathodes for Solar Hydrogen Production. *Nanoscale* **2020**, *12*, 7766−7775.
(108) Ellis, A. B.; Kaiser, S. W.; Bolts, J. M.; Wrighton, M. S. Study of n-Type Semiconducting Cadmium Chalcogenide-Based Photoelectrochemical Cells Employing Polychalcogenide Electrolytes. *J. Am. Chem. Soc.* **1977**, *99*, 2839−2848.
(109) Knöppel, J.; Zhang, S.; Speck, F. D.; Mayrhofer, K. J. J.; Scheu, C.; Cherevko, S. Time-Resolved Analysis of Dissolution Phenomena in Photoelectrochemistry - A Case Study of WO_3 Photocorrosion. *Electrochem. Commun.* **2018**, *96*, 53−56.
(110) Zhang, S.; Rohloff, M.; Kasian, O.; Mingers, A. M.; Mayrhofer, K. J. J.; Fischer, A.; Scheu, C.; Cherevko, S. Dissolution of $BiVO_4$ Photoanodes Revealed by Time-Resolved Measurements under Photoelectrochemical Conditions. *J. Phys. Chem. C* **2019**, *123*, 23410−23418.
(111) Wu, K.; Liang, G.; Shang, Q.; Ren, Y.; Kong, D.; Lian, T. Ultrafast Interfacial Electron and Hole Transfer from $CsPbBr_3$ Perovskite Quantum Dots. *J. Am. Chem. Soc.* **2015**, *137*, 12792−12795.
(112) Hsu, H.-Y.; Ji, L.; Ahn, H. S.; Zhao, J.; Yu, E. T.; Bard, A. J. A Liquid Junction Photoelectrochemical Solar Cell Based on p-Type $MeNH_3PbI_3$ Perovskite with 1.05 V Open-Circuit Photovoltage. *J. Am. Chem. Soc.* **2015**, *137*, 14758−14764.
(113) Zhang, Y.-X.; Wang, H.-Y.; Zhang, Z.-Y.; Zhang, Y.; Sun, C.; Yue, Y.-Y.; Wang, L.; Chen, Q.-D.; Sun, H.-B. Photoluminescence Quenching of Inorganic Cesium Lead Halides Perovskite Quantum Dots ($CsPbX_3$) by Electron/Hole Acceptor. *Phys. Chem. Chem. Phys.* **2017**, *19*, 1920−1926.
(114) DuBose, J. T.; Kamat, P. V. Surface Chemistry Matters. How Ligands Influence Excited State Interactions between $CsPbBr_3$ and Methyl Viologen. *J. Phys. Chem. C* **2020**, *124*, 12990−12998.
(115) Kobosko, S. M.; DuBose, J. T.; Kamat, P. V. Perovskite Photocatalysis. Methyl Viologen Induces Unusually Long-Lived Charge Carrier Separation in $CsPbBr_3$ Nanocrystals. *ACS Energy Lett.* **2020**, *5*, 221−223.
(116) Hsu, H.-Y.; Ji, L.; Du, M.; Zhao, J.; Yu, E. T.; Bard, A. J. Optimization of Lead-Free Organic-Inorganic Tin(II) Halide Perovskite Semiconductors by Scanning Electrochemical Microscopy. *Electrochim. Acta* **2016**, *220*, 205−210.
(117) Yang, M.-Z.; Xu, Y.-F.; Liao, J.-F.; Wang, X.-D.; Chen, H.-Y.; Kuang, D.-B. Constructing $CsPbBr_xI_{3-x}$ Nanocrystal/Carbon Nanotube Composites with Improved Charge Transfer and Light Harvesting for Enhanced Photoelectrochemical Activity. *J. Mater. Chem. A* **2019**, *7*, 5409−5415.
(118) Liao, J.-F.; Xu, Y.-F.; Wang, X.-D.; Chen, H.-Y.; Kuang, D.-B. $CsPbBr_3$ Nanocrystal/MO_2 (M = Si, Ti, Sn) Composites: Insight into Charge-Carrier Dynamics and Photoelectrochemical Applications. *ACS Appl. Mater. Interfaces* **2018**, *10* (49), 42301−42309.
(119) Wang, Q.; Tao, L.; Jiang, X.; Wang, M.; Shen, Y. Graphene Oxide Wrapped $CH_3NH_3PbBr_3$ Perovskite Quantum Dots Hybrid for Photoelectrochemical CO_2 Reduction in Organic Solvents. *Appl. Surf. Sci.* **2019**, *465*, 607−613.
(120) Xu, Y.; Wang, X.; Liao, J.; Chen, B.; Chen, H.; Kuang, D. Amorphous-TiO_2 -Encapsulated $CsPbBr_3$ Nanocrystal Composite Photocatalyst with Enhanced Charge Separation and CO_2 Fixation. *Adv. Mater. Interfaces* **2018**, *5*, 1801015.
(121) Li, Z.-J.; Hofman, E.; Li, J.; Davis, A. H.; Tung, C.-H.; Wu, L.-Z.; Zheng, W. Photoelectrochemically Active and Environmentally Stable $CsPbBr_3/TiO_2$ Core/Shell Nanocrystals. *Adv. Funct. Mater.* **2018**, *28*, 1704288.
(122) Huang, W.; Manser, J. S.; Kamat, P. V.; Ptasinska, S. Evolution of Chemical Composition, Morphology, and Photovoltaic Efficiency of $CH_3NH_3PbI_3$ Perovskite under Ambient Conditions. *Chem. Mater.* **2016**, *28*, 303−311.
(123) Hsu, H.-Y.; Ji, L.; Du, M.; Zhao, J.; Yu, E. T.; Bard, A. J. Optimization of $PbI_2/MAPbI_3$ Perovskite Composites by Scanning Electrochemical Microscopy. *J. Phys. Chem. C* **2016**, *120*, 19890−19895.
(124) Hsu, H.-Y.; Ji, L.; Zhang, C.; Mak, C. H.; Liu, R.; Wang, T.; Zou, X.; Leu, S.-Y.; Yu, E. T. Ultra-Stable 2D Layered Methylammonium Cadmium Trihalide Perovskite Photoelectrodes. *J. Mater. Chem. C* **2018**, *6*, 11552−11560.
(125) Guo, S.-H.; Zhou, J.; Zhao, X.; Sun, C.-Y.; You, S.-Q.; Wang, X.-L.; Su, Z.-M. Enhanced CO_2 Photoreduction via Tuning Halides in Perovskites. *J. Catal.* **2019**, *369*, 201−208.
(126) Wan, S.; Ou, M.; Zhong, Q.; Wang, X. Perovskite-Type $CsPbBr_3$ Quantum Dots/UiO-66(NH_2) Nanojunction as Efficient Visible-Light-Driven Photocatalyst for CO_2 Reduction. *Chem. Eng. J.* **2019**, *358*, 1287−1295.
(127) Mu, Y.; Zhang, W.; Guo, X.; Dong, G.; Zhang, M.; Lu, T. Water-Tolerant Lead Halide Perovskite Nanocrystals as Efficient Photocatalysts for Visible-Light-Driven CO 2 Reduction in Pure Water. *ChemSusChem* **2019**, *12* (21), 4769−4774.
(128) Cardenas-Morcoso, D.; Gualdrón-Reyes, A. F.; Ferreira Vitoreti, A. B.; García-Tecedor, M.; Yoon, S. J.; Solis de la Fuente, M.; Mora-Seró, I.; Gimenez, S. Photocatalytic and Photoelectrochemical Degradation of Organic Compounds with All-Inorganic Metal Halide Perovskite Quantum Dots. *J. Phys. Chem. Lett.* **2019**, *10*, 630−636.
(129) Knight, A. J.; Herz, L. M. Preventing Phase Segregation in Mixed-Halide Perovskites: A Perspective. *Energy Environ. Sci.* **2020**, *13*, 2024−2046.
(130) Bischak, C. G.; Hetherington, C. L.; Wu, H.; Aloni, S.; Ogletree, D. F.; Limmer, D. T.; Ginsberg, N. S. Origin of Reversible Photoinduced Phase Separation in Hybrid Perovskites. *Nano Lett.* **2017**, *17*, 1028−1033.
(131) Barker, A. J.; Sadhanala, A.; Deschler, F.; Gandini, M.; Senanayak, S. P.; Pearce, P. M.; Mosconi, E.; Pearson, A. J.; Wu, Y.; Srimath Kandada, A. R.; Leijtens, T.; De Angelis, F.; Dutton, S. E. S. E.; Petrozza, A.; Friend, R. H. Defect-Assisted Photoinduced Halide Segregation in Mixed-Halide Perovskite Thin Films. *ACS Energy Lett.* **2017**, *2*, 1416−1424.
(132) Knight, A. J.; Wright, A. D.; Patel, J. B.; McMeekin, D. P.; Snaith, H. J.; Johnston, M. B.; Herz, L. M. Electronic Traps and Phase Segregation in Lead Mixed-Halide Perovskite. *ACS Energy Lett.* **2019**, *4*, 75−84.
(133) Bischak, C. G.; Wong, A. B.; Lin, E.; Limmer, D. T.; Yang, P.; Ginsberg, N. S. Tunable Polaron Distortions Control the Extent of Halide Demixing in Lead Halide Perovskites. *J. Phys. Chem. Lett.* **2018**, *9*, 3998−4005.
(134) Miyata, K.; Meggiolaro, D.; Trinh, M. T.; Joshi, P. P.; Mosconi, E.; Jones, S. C.; De Angelis, F.; Zhu, X.-Y. Large Polarons in Lead Halide Perovskites. *Sci. Adv.* **2017**, *3*, No. e1701217.
(135) Ravi, V. K.; Scheidt, R. A.; Nag, A.; Kuno, M.; Kamat, P. V. To Exchange or Not to Exchange. Suppressing Anion Exchange in Cesium Lead Halide Perovskites with $PbSO_4$ -Oleate Capping. *ACS Energy Lett.* **2018**, *3*, 1049−1055.
(136) Samu, G. F.; Janáky, C.; Kamat, P. V. A Victim of Halide Ion Segregation. How Light Soaking Affects Solar Cell Performance of Mixed Halide Lead Perovskites. *ACS Energy Lett.* **2017**, *2*, 1860−1861.
(137) Shallcross, R. C.; Zheng, Y.; Saavedra, S. S.; Armstrong, N. R. Determining Band-Edge Energies and Morphology-Dependent Stability of Formamidinium Lead Perovskite Films Using Spectroelectrochemistry and Photoelectron Spectroscopy. *J. Am. Chem. Soc.* **2017**, *139*, 4866−4878.
(138) Gomes, W. P.; Lingier, S.; Vanmaekelbergh, D. Anodic Stabilization and Decomposition Mechanisms in Semiconductor

https://dx.doi.org/10.1021/jacs.0c10348
J. Am. Chem. Soc. 2020, 142, 21595−21614

(Photo)-Electrochemistry. *J. Electroanal. Chem. Interfacial Electrochem.* **1989**, *269*, 237−249.
(139) Vanmaekelbergh, D.; Gomes, W. P.; Cardon, F. Studies on the n-GaAs Photoanode in Aqueous Electrolytes. 1. Behaviour of the Photocurrent in the Presence of a Stabilizing Agent. *Berichte der Bunsengesellschaft für Phys. Chemie* **1985**, *89*, 987−994.
(140) Vanmaekelbergh, D.; Kelly, J. J.; Lingier, S.; Gomes, W. P. Electron Excitation and Chemical Steps during Anodic Decomposition of n-GaAs Electrodes: A Hole Injection Study. *Berichte der Bunsengesellschaft für Phys. Chemie* **1988**, *92*, 1068−1072.
(141) Frese, K. W.; Madou, M. J.; Morrison, S. R. Investigation of Photoelectrochemical Corrosion of Semiconductors II. Kinetic Analysis of Corrosion-Competition Reactions on n-GaAs. *J. Electrochem. Soc.* **1981**, *128*, 1527−1531.
(142) Frese, K. W.; Madou, M. J.; Morrison, S. R. Investigation of Photoelectrochemical Corrosion of Semiconductors III. Effects of Metal Layer on Stability of GaAs. *J. Electrochem. Soc.* **1981**, *128*, 1939−1943.
(143) Frese, K. W.; Canfield, D. Photocorrosion of n-CdSe in Sulfide Electrolytes. *J. Electrochem. Soc.* **1985**, *132*, 1649−1655.
(144) Reineke, R.; Memming, R. Comparability of Redox Reactions at n- and p-Type Semiconductor Electrodes. 2. Electrochemical Overpotential and Recombination in View of the Quasi-Fermi Level Concept. *J. Phys. Chem.* **1992**, *96*, 1317−1323.
(145) Vanmaekelbergh, D.; Gomes, W. P.; Cardon, F. Study of Stabilization and Surface Recombination on n-GaP Photoelectrodes: Mechanisms and Interrelation. *J. Electrochem. Soc.* **1982**, *129*, 546−550.
(146) Frese, K. W. Electrochemical Studies of Photocorrosion of n-CdSe. *J. Electrochem. Soc.* **1983**, *130*, 28−33.
(147) Peter, L. M.; Borazio, A. M.; Lewerenz, H. J.; Stumper, J. Photocurrent Multiplication during Photodissolution of n-Si in NH_4F: Deconvolution of Electron Injection Steps by Intensity Modulated Photocurrent Spectroscopy. *J. Electroanal. Chem. Interfacial Electrochem.* **1990**, *290*, 229−248.
(148) Fermín, D. J.; Ponomarev, E. A.; Peter, L. M. A Kinetic Study of CdS Photocorrosion by Intensity Modulated Photocurrent and Photoelectrochemical Impedance Spectroscopy. *J. Electroanal. Chem.* **1999**, *473*, 192−203.
(149) Favaro, M.; Abdi, F. F.; Lamers, M.; Crumlin, E. J.; Liu, Z.; van de Krol, R.; Starr, D. E. Light-Induced Surface Reactions at the Bismuth Vanadate/Potassium Phosphate Interface. *J. Phys. Chem. B* **2018**, *122*, 801−809.
(150) Shavorskiy, A.; Ye, X.; Karslıoğlu, O.; Poletayev, A. D.; Hartl, M.; Zegkinoglou, I.; Trotochaud, L.; Nemšák, S.; Schneider, C. M.; Crumlin, E. J.; Axnanda, S.; Liu, Z.; Ross, P. N.; Chueh, W.; Bluhm, H. Direct Mapping of Band Positions in Doped and Undoped Hematite during Photoelectrochemical Water Splitting. *J. Phys. Chem. Lett.* **2017**, *8*, 5579−5586.
(151) Lebedev, M. V.; Calvet, W.; Mayer, T.; Jaegermann, W. Photoelectrochemical Processes at N-GaAs(100)/Aqueous HCl Electrolyte Interface: A Synchrotron Photoemission Spectroscopy Study of Emersed Electrodes. *J. Phys. Chem. C* **2014**, *118*, 12774−12781.
(152) Lebedev, M. V.; Calvet, W.; Kaiser, B.; Jaegermann, W. Synchrotron Photoemission Spectroscopy Study of p-$GaInP_2$(100) Electrodes Emersed from Aqueous HCl Solution under Cathodic Conditions. *J. Phys. Chem. C* **2017**, *121*, 8889−8901.
(153) de Tacconi, N. R.; Rajeshwar, K. Anodic Growth and Interphasial Photoelectrochemistry of Cadmium Sulfide Thin Films as Probed by Laser Raman Spectroscopy. *J. Phys. Chem.* **1993**, *97*, 6504−6508.
(154) Sourisseau, C.; Cruege, F.; Gorochov, O. In-Situ Raman Investigation of Photo-Corrosion Processes at p- and n-Type WS_2 Electrodes in Acid Solutions. *J. Electroanal. Chem. Interfacial Electrochem.* **1991**, *308*, 239−253.
(155) Awatani, T.; McQuillan, A. J. Adsorbed Thiosulfate Intermediate of Cadmium Sulfide Aqueous Photocorrosion Detected and Characterized by in Situ Infrared Spectroscopy. *J. Phys. Chem. B* **1998**, *102*, 4110−4113.
(156) de Tacconi, N. R.; Myung, N.; Rajeshwar, K. Overlayer Formation in the n-CdSe/$[Fe(CN)_6]^{4-/3-}$ Photoelectrochemical System As Probed by Laser Raman Spectroscopy and Electrochemical Quartz Crystal Microgravimetry. *J. Phys. Chem.* **1995**, *99*, 6103−6109.
(157) Žídek, K.; Zheng, K.; Chábera, P.; Abdellah, M.; Pullerits, T. Quantum Dot Photodegradation Due to CdSe-ZnO Charge Transfer: Transient Absorption Study. *Appl. Phys. Lett.* **2012**, *100*, 243111.
(158) Scheidt, R. A.; Samu, G. F.; Janáky, C.; Kamat, P. V. Modulation of Charge Recombination in $CsPbBr_3$ Perovskite Films with Electrochemical Bias. *J. Am. Chem. Soc.* **2018**, *140*, 86−89.
(159) Hines, D. A.; Becker, M. A.; Kamat, P. V. Photoinduced Surface Oxidation and Its Effect on the Exciton Dynamics of CdSe Quantum Dots. *J. Phys. Chem. C* **2012**, *116*, 13452−13457.
(160) Žídek, K.; Zheng, K.; Abdellah, M.; Chábera, P.; Pullerits, T.; Tachyia, M. Simultaneous Creation and Recovery of Trap States on Quantum Dots in a Photoirradiated CdSe-ZnO System. *J. Phys. Chem. C* **2014**, *118*, 27567−27573.
(161) Allongue, P.; Cachet, H. Photocapacitance Study of n-GaAs/Electrolyte Interfaces. *Berichte der Bunsengesellschaft für Phys. Chemie* **1987**, *91*, 386−390.
(162) Allongue, P.; Cachet, H. Steady State Photocapacitance Study of Semiconductor/Aqueous Electrolyte Junctions: I. Interest and Difficulties in the Case of n-GaAs. *Berichte der Bunsengesellschaft für Phys. Chemie* **1988**, *92*, 566−572.
(163) Allongue, P. Steady State Photocapacitance Study of Semiconductor/Electrolyte Junctions II. Surface State Distribution and Charge Transfer Mechanisms. *Berichte der Bunsengesellschaft für Phys. Chemie* **1988**, *92*, 895−903.
(164) Allongue, P.; Tenne, R. Primary Reactions in the Photocorrosion of CdSe Through Photocapacitance Measurements. *J. Electrochem. Soc.* **1991**, *138*, 261−268.
(165) Vanmaekelbergh, D.; Gomes, W. P.; Cardon, F. Studies on the n-GaAs Photoanode in Aqueous Electrolytes. 2. Differential Capacitance Behaviour. *Berichte der Bunsengesellschaft für Phys. Chemie* **1985**, *89*, 994−998.
(166) Kühne, H.-M.; Tributsch, H. Energetics and Dynamics of the Interface of RuS_2 and Implications for Photoelectrolysis of Water. *J. Electroanal. Chem. Interfacial Electrochem.* **1986**, *201*, 263−282.
(167) Lincot, D.; Vedel, J. Recombination and Charge Transfer at the Illuminated n-CdTe/Electrolyte Interface. *J. Electroanal. Chem. Interfacial Electrochem.* **1987**, *220*, 179−200.
(168) de Wit, A. R.; Vanmaekelbergh, D.; Kelly, J. J. A Study of the Photoanodic Dissolution of CdS with Electrical and Opto-Electrical Impedance Spectroscopy. *J. Electrochem. Soc.* **1992**, *139*, 2508−2513.
(169) Vaiunaekelbergh, D.; Gomes, W. P.; Cardon, F. Studies on the n-GaAs Photoanode in Aqueous Electrolytes. 3. Recombination Resistance. *Berichte der Bunsengesellschaft für Phys. Chemie* **1986**, *90*, 431−434.
(170) Myung, N.; Wei, C.; de Tacconi, N. R.; Rajeshwar, K. Photoelectrochemical Quartz Crystal Microgravimetry. Development and Use as an in Situ Photoelectrode Corrosion and Stabilization Probe. *J. Electroanal. Chem.* **1993**, *359*, 307−313.
(171) Erné, B. H.; et al. Surface Composition of n-GaAs Cathodes during Hydrogen Evolution Characterized by In Situ Ultraviolet-Visible Ellipsometry and In Situ Infrared Spectroscopy. *J. Electrochem. Soc.* **1998**, *145*, 447−456.
(172) Balog, Á.; Samu, G. F.; Kamat, P. V.; Janáky, C. Optoelectronic Properties of CuI Photoelectrodes. *J. Phys. Chem. Lett.* **2019**, *10*, 259−264.
(173) Balko, B. A.; Richmond, G. L. Corrosion-Induced Surface States on n-Gallium Arsenide as Studied by Photoluminescence versus Voltage Scans and Luminescence Decays. *J. Phys. Chem.* **1993**, *97*, 9002−9008.
(174) Abshere, T. A.; Richmond, G. L. Picosecond Photoluminescence Study of the n-GaAs(100)/Methanol Interface in a Photoelectrochemical Cell. *J. Phys. Chem. B* **1999**, *103*, 7911−7919.
(175) Abshere, T. A.; Richmond, G. L. Corrosion, Passivation, and the Effect of Water Addition on an n-GaAs(100)/Methanol Photoelectrochemical Cell. *J. Phys. Chem. B* **2000**, *104*, 1602−1609.

https://dx.doi.org/10.1021/jacs.0c10348
J. Am. Chem. Soc. 2020, 142, 21595−21614

(176) Lai, J.; Yuan, D.; Huang, P.; Zhang, J.; Su, J.-J.; Tian, Z.-W.; Zhan, D. Kinetic Investigation on the Photoetching Reaction of n-Type GaAs by Scanning Electrochemical Microscopy. *J. Phys. Chem. C* **2016**, *120*, 16446−16452.
(177) Manser, J. S.; Christians, J. A.; Kamat, P. V. Intriguing Optoelectronic Properties of Metal Halide Perovskites. *Chem. Rev.* **2016**, *116*, 12956−13008.
(178) McLeod, J. A.; Liu, L. Prospects for Mitigating Intrinsic Organic Decomposition in Methylammonium Lead Triiodide Perovskite. *J. Phys. Chem. Lett.* **2018**, *9*, 2411−2417.
(179) Schutt, K.; Nayak, P. K.; Ramadan, A. J.; Wenger, B.; Lin, Y.; Snaith, H. J. Overcoming Zinc Oxide Interface Instability with a Methylammonium-Free Perovskite for High-Performance Solar Cells. *Adv. Funct. Mater.* **2019**, *29*, 1900466.
(180) McMeekin, D. P.; Sadoughi, G.; Rehman, W.; Eperon, G. E.; Saliba, M.; Horantner, M. T.; Haghighirad, A.; Sakai, N.; Korte, L.; Rech, B.; Johnston, M. B.; Herz, L. M.; Snaith, H. J. A Mixed-Cation Lead Mixed-Halide Perovskite Absorber for Tandem Solar Cells. *Science* **2016**, *351* (6269), 151−155.
(181) Saliba, M.; Matsui, T.; Seo, J.-Y.; Domanski, K.; Correa-Baena, J.-P.; Nazeeruddin, M. K.; Zakeeruddin, S. M.; Tress, W.; Abate, A.; Hagfeldt, A.; Grätzel, M. Cesium-Containing Triple Cation Perovskite Solar Cells: Improved Stability, Reproducibility and High Efficiency. *Energy Environ. Sci.* **2016**, *9*, 1989−1997.
(182) García-Fernández, A.; Juarez-Perez, E. J.; Castro-García, S.; Sánchez-Andújar, M.; Ono, L. K.; Jiang, Y.; Qi, Y. Benchmarking Chemical Stability of Arbitrarily Mixed 3D Hybrid Halide Perovskites for Solar Cell Applications. *Small Methods* **2018**, *2*, 1800242.
(183) Jeon, N. J.; Noh, J. H.; Yang, W. S.; Kim, Y. C.; Ryu, S.; Seo, J.; Seok, S., II Compositional Engineering of Perovskite Materials for High-Performance Solar Cells. *Nature* **2015**, *517*, 476−480.
(184) Pont, S.; Bryant, D.; Lin, C.-T.; Aristidou, N.; Wheeler, S.; Ma, X.; Godin, R.; Haque, S. A.; Durrant, J. R. Tuning $CH_3NH_3Pb(I_{1-x}Br_x)_3$ Perovskite Oxygen Stability in Thin Films and Solar Cells. *J. Mater. Chem. A* **2017**, *5*, 9553−9560.
(185) Noh, J. H.; Im, S. H.; Heo, J. H.; Mandal, T. N.; Seok, S., II Chemical Management for Colorful, Efficient, and Stable Inorganic-Organic Hybrid Nanostructured Solar Cells. *Nano Lett.* **2013**, *13*, 1764−1769.
(186) Xu, J.; Boyd, C. C.; Yu, Z. J.; Palmstrom, A. F.; Witter, D. J.; Larson, B. W.; France, R. M.; Werner, J.; Harvey, S. P.; Wolf, E. J.; Weigand, W.; Manzoor, S.; van Hest, M. F. A. M.; Berry, J. J.; Luther, J. M.; Holman, Z. C.; McGehee, M. D. Triple-Halide Wide-Band Gap Perovskites with Suppressed Phase Segregation for Efficient Tandems. *Science* **2020**, *367*, 1097−1104.
(187) Cho, J.; Kamat, P. V. How Chloride Suppresses Photoinduced Phase Segregation in Mixed Halide Perovskites. *Chem. Mater.* **2020**, *32*, 6206−6212.
(188) Yu, H.; Wang, F.; Xie, F.; Li, W.; Chen, J.; Zhao, N. The Role of Chlorine in the Formation Process of "$CH_3NH_3PbI_{3-x}Cl_x$" Perovskite. *Adv. Funct. Mater.* **2014**, *24*, 7102−7108.
(189) Medjahed, A. A.; Dally, P.; Zhou, T.; Lemaitre, N.; Djurado, D.; Reiss, P.; Pouget, S. Unraveling the Formation Mechanism and Ferroelastic Behavior of $MAPbI_3$ Perovskite Thin Films Prepared in the Presence of Chloride. *Chem. Mater.* **2020**, *32*, 3346−3357.
(190) Chen, B.; Yu, Z.; Liu, K.; Zheng, X.; Liu, Y.; Shi, J.; Spronk, D.; Rudd, P. N.; Holman, Z.; Huang, J. Grain Engineering for Perovskite/Silicon Monolithic Tandem Solar Cells with Efficiency of 25.4%. *Joule* **2019**, *3*, 177−190.
(191) Zhang, H.; Lv, Y.; Wang, J.; Ma, H.; Sun, Z.; Huang, W. Influence of Cl Incorporation in Perovskite Precursor on the Crystal Growth and Storage Stability of Perovskite Solar Cells. *ACS Appl. Mater. Interfaces* **2019**, *11*, 6022−6030.
(192) Ma, D.; Todorović, P.; Meshkat, S.; Saidaminov, M. I.; Wang, Y.-K.; Chen, B.; Li, P.; Scheffel, B.; Quintero-Bermudez, R.; Fan, J. Z.; Dong, Y.; Sun, B.; Xu, C.; Zhou, C.; Hou, Y.; Li, X.; Kang, Y.; Voznyy, O.; Lu, Z.-H.; Ban, D.; Sargent, E. H. Chloride Insertion-Immobilization Enables Bright, Narrowband, and Stable Blue-Emitting Perovskite Diodes. *J. Am. Chem. Soc.* **2020**, *142*, 5126−5134.
(193) Wang, S.; Liu, G.; Wang, L. Crystal Facet Engineering of Photoelectrodes for Photoelectrochemical Water Splitting. *Chem. Rev.* **2019**, *119*, 5192−5247.
(194) Chen, Z.; Turedi, B.; Alsalloum, A. Y.; Yang, C.; Zheng, X.; Gereige, I.; AlSaggaf, A.; Mohammed, O. F.; Bakr, O. M. Single-Crystal $MAPbI_3$ Perovskite Solar Cells Exceeding 21% Power Conversion Efficiency. *ACS Energy Lett.* **2019**, *4*, 1258−1259.
(195) Alsalloum, A. Y.; Turedi, B.; Zheng, X.; Mitra, S.; Zhumekenov, A. A.; Lee, K. J.; Maity, P.; Gereige, I.; AlSaggaf, A.; Roqan, I. S.; Mohammed, O. F.; Bakr, O. M. Low-Temperature Crystallization Enables 21.9% Efficient Single-Crystal $MAPbI_3$ Inverted Perovskite Solar Cells. *ACS Energy Lett.* **2020**, *5*, 657−662.
(196) Ortiz-Cervantes, C.; Carmona-Monroy, P.; Solis-Ibarra, D. Two-Dimensional Halide Perovskites in Solar Cells: 2D or Not 2D? *ChemSusChem* **2019**, *12*, 1560−1575.
(197) Stoumpos, C. C.; Cao, D. H.; Clark, D. J.; Young, J.; Rondinelli, J. M.; Jang, J. I.; Hupp, J. T.; Kanatzidis, M. G. Ruddlesden-Popper Hybrid Lead Iodide Perovskite 2D Homologous Semiconductors. *Chem. Mater.* **2016**, *28*, 2852−2867.
(198) Smith, I. C.; Hoke, E. T.; Solis-Ibarra, D.; McGehee, M. D.; Karunadasa, H. I. A Layered Hybrid Perovskite Solar-Cell Absorber with Enhanced Moisture Stability. *Angew. Chem., Int. Ed.* **2014**, *53*, 11232−11235.
(199) Cao, D. H.; Stoumpos, C. C.; Farha, O. K.; Hupp, J. T.; Kanatzidis, M. G. 2D Homologous Perovskites as Light-Absorbing Materials for Solar Cell Applications. *J. Am. Chem. Soc.* **2015**, *137*, 7843−7850.
(200) Grancini, G.; Roldán-Carmona, C.; Zimmermann, I.; Mosconi, E.; Lee, X.; Martineau, D.; Narbey, S.; Oswald, F.; De Angelis, F.; Graetzel, M.; Nazeeruddin, M. K. One-Year Stable Perovskite Solar Cells by 2D/3D Interface Engineering. *Nat. Commun.* **2017**, *8*, 15684.
(201) Quan, L. N.; Yuan, M.; Comin, R.; Voznyy, O.; Beauregard, E. M.; Hoogland, S.; Buin, A.; Kirmani, A. R.; Zhao, K.; Amassian, A.; Kim, D. H.; Sargent, E. H. Ligand-Stabilized Reduced-Dimensionality Perovskites. *J. Am. Chem. Soc.* **2016**, *138*, 2649−2655.
(202) Zhang, F.; Zhu, K. Additive Engineering for Efficient and Stable Perovskite Solar Cells. *Adv. Energy Mater.* **2020**, *10*, 1902579.
(203) Wang, S.; Cao, H.; Liu, X.; Liu, Y.; Tao, T.; Sun, J.; Zhang, M. Strontium Chloride-Passivated Perovskite Thin Films for Efficient Solar Cells with Power Conversion Efficiency over 21% and Superior Stability. *ACS Appl. Mater. Interfaces* **2020**, *12*, 3661−3669.
(204) Tang, Z.; Uchida, S.; Bessho, T.; Kinoshita, T.; Wang, H.; Awai, F.; Jono, R.; Maitani, M. M.; Nakazaki, J.; Kubo, T.; Segawa, H. Modulations of Various Alkali Metal Cations on Organometal Halide Perovskites and Their Influence on Photovoltaic Performance. *Nano Energy* **2018**, *45*, 184−192.
(205) Kim, Y. C.; Jeon, N. J.; Noh, J. H.; Yang, W. S.; Seo, J.; Yun, J. S.; Ho-Baillie, A.; Huang, S.; Green, M. A.; Seidel, J.; Ahn, T. K.; Seok, S., II Beneficial Effects of PbI_2 Incorporated in Organo-Lead Halide Perovskite Solar Cells. *Adv. Energy Mater.* **2016**, *6*, 1502104.
(206) Zheng, X.; Chen, B.; Dai, J.; Fang, Y.; Bai, Y.; Lin, Y.; Wei, H.; Zeng, X. C.; Huang, J. Defect Passivation in Hybrid Perovskite Solar Cells Using Quaternary Ammonium Halide Anions and Cations. *Nat. Energy* **2017**, *2*, 17102.
(207) Zheng, K.; Chen, Y.; Sun, Y.; Chen, J.; Chábera, P.; Schaller, R.; Al-Marri, M. J.; Canton, S. E.; Liang, Z.; Pullerits, T. Inter-Phase Charge and Energy Transfer in Ruddlesden-Popper 2D Perovskites: Critical Role of the Spacing Cations. *J. Mater. Chem. A* **2018**, *6*, 6244−6250.
(208) Jiang, Q.; Zhao, Y.; Zhang, X.; Yang, X.; Chen, Y.; Chu, Z.; Ye, Q.; Li, X.; Yin, Z.; You, J. Surface Passivation of Perovskite Film for Efficient Solar Cells. *Nat. Photonics* **2019**, *13*, 460−466.
(209) Li, N.; Zhu, Z.; Dong, Q.; Li, J.; Yang, Z.; Chueh, C.-C.; Jen, A. K.-Y.; Wang, L. Enhanced Moisture Stability of Cesium-Containing Compositional Perovskites by a Feasible Interfacial Engineering. *Adv. Mater. Interfaces* **2017**, *4*, 1700598.
(210) Guo, P.; Ye, Q.; Yang, X.; Zhang, J.; Xu, F.; Shchukin, D.; Wei, B.; Wang, H. Surface & Grain Boundary Co-Passivation by Fluorocarbon Based Bifunctional Molecules for Perovskite Solar Cells with Efficiency over 21%. *J. Mater. Chem. A* **2019**, *7*, 2497−2506.

https://dx.doi.org/10.1021/jacs.0c10348
J. Am. Chem. Soc. 2020, 142, 21595−21614

(211) Wang, Q.; Chen, B.; Liu, Y.; Deng, Y.; Bai, Y.; Dong, Q.; Huang, J. Scaling Behavior of Moisture-Induced Grain Degradation in Polycrystalline Hybrid Perovskite Thin Films. *Energy Environ. Sci.* **2017**, *10*, 516−522.
(212) Nandjou, F.; Haussener, S. Degradation in Photoelectrochemical Devices: Review with an Illustrative Case Study. *J. Phys. D: Appl. Phys.* **2017**, *50*, 124002.
(213) Da, P.; Cha, M.; Sun, L.; Wu, Y.; Wang, Z.-S.; Zheng, G. High-Performance Perovskite Photoanode Enabled by Ni Passivation and Catalysis. *Nano Lett.* **2015**, *15*, 3452−3457.
(214) Hoang, M. T.; Pham, N. D.; Han, J. H.; Gardner, J. M.; Oh, I. Integrated Photoelectrolysis of Water Implemented On Organic Metal Halide Perovskite Photoelectrode. *ACS Appl. Mater. Interfaces* **2016**, *8*, 11904−11909.
(215) Wang, C.; Yang, S.; Chen, X.; Wen, T.; Yang, H. G. Surface-Functionalized Perovskite Films for Stable Photoelectrochemical Water Splitting. *J. Mater. Chem. A* **2017**, *5*, 910−913.
(216) Zhang, H.; Yang, Z.; Yu, W.; Wang, H.; Ma, W.; Zong, X.; Li, C. A Sandwich-Like Organolead Halide Perovskite Photocathode for Efficient and Durable Photoelectrochemical Hydrogen Evolution in Water. *Adv. Energy Mater.* **2018**, *8*, 1800795.
(217) Crespo-Quesada, M.; Pazos-Outón, L. M.; Warnan, J.; Kuehnel, M. F.; Friend, R. H.; Reisner, E. Metal-Encapsulated Organolead Halide Perovskite Photocathode for Solar-Driven Hydrogen Evolution in Water. *Nat. Commun.* **2016**, *7*, 12555.
(218) Nam, S.; Mai, C. T. K.; Oh, I. Ultrastable Photoelectrodes for Solar Water Splitting Based on Organic Metal Halide Perovskite Fabricated by Lift-Off Process. *ACS Appl. Mater. Interfaces* **2018**, *10*, 14659−14664.
(219) Gao, L.-F.; Luo, W.-J.; Yao, Y.-F.; Zou, Z.-G. An All-Inorganic Lead Halide Perovskite-Based Photocathode for Stable Water Reduction. *Chem. Commun.* **2018**, *54*, 11459−11462.
(220) Ahmad, S.; Sadhanala, A.; Hoye, R. L. Z.; Andrei, V.; Modarres, M. H.; Zhao, B.; Rongé, J.; Friend, R.; De Volder, M. Triple-Cation-Based Perovskite Photocathodes with AZO Protective Layer for Hydrogen Production Applications. *ACS Appl. Mater. Interfaces* **2019**, *11*, 23198−23206.
(221) Andrei, V.; Hoye, R. L. Z.; Crespo-Quesada, M.; Bajada, M.; Ahmad, S.; De Volder, M.; Friend, R.; Reisner, E. Scalable Triple Cation Mixed Halide Perovskite-$BiVO_4$ Tandems for Bias-Free Water Splitting. *Adv. Energy Mater.* **2018**, *8*, 1801403.
(222) Chen, J.; Yin, J.; Zheng, X.; Ait Ahsaine, H.; Zhou, Y.; Dong, C.; Mohammed, O. F.; Takanabe, K.; Bakr, O. M. Compositionally Screened Eutectic Catalytic Coatings on Halide Perovskite Photocathodes for Photoassisted Selective CO_2 Reduction. *ACS Energy Lett.* **2019**, *4*, 1279−1286.
(223) Edwardes Moore, E.; Andrei, V.; Zacarias, S.; Pereira, I. A. C.; Reisner, E. Integration of a Hydrogenase in a Lead Halide Perovskite Photoelectrode for Tandem Solar Water Splitting. *ACS Energy Lett.* **2020**, *5*, 232−237.
(224) Andrei, V.; Reuillard, B.; Reisner, E. Bias-Free Solar Syngas Production by Integrating a Molecular Cobalt Catalyst with Perovskite-$BiVO_4$ Tandems. *Nat. Mater.* **2020**, *19*, 189.
(225) Rahaman, M.; Andrei, V.; Pornrungroj, C.; Wright, D.; Baumberg, J. J.; Reisner, E. Selective CO Production from Aqueous CO_2 Using a $Cu_{96}In_4$ Catalyst and Its Integration into a Bias-Free Solar Perovskite-$BiVO_4$ Tandem Device. *Energy Environ. Sci.* **2020**, *13*, 3536−3543.
(226) Tao, R.; Sun, Z.; Li, F.; Fang, W.; Xu, L. Achieving Organic Metal Halide Perovskite into a Conventional Photoelectrode: Outstanding Stability in Aqueous Solution and High-Efficient Photoelectrochemical Water Splitting. *ACS Appl. Energy Mater.* **2019**, *2*, 1969−1976.
(227) Poli, I.; Hintermair, U.; Regue, M.; Kumar, S.; Sackville, E. V.; Baker, J.; Watson, T. M.; Eslava, S.; Cameron, P. J. Graphite-Protected $CsPbBr_3$ Perovskite Photoanodes Functionalised with Water Oxidation Catalyst for Oxygen Evolution in Water. *Nat. Commun.* **2019**, *10*, 2097.
(228) Kim, I. S.; Pellin, M. J.; Martinson, A. B. F. Acid-Compatible Halide Perovskite Photocathodes Utilizing Atomic Layer Deposited TiO_2 for Solar-Driven Hydrogen Evolution. *ACS Energy Lett.* **2019**, *4*, 293−298.
(229) Zardetto, V.; Williams, B. L.; Perrotta, A.; Di Giacomo, F.; Verheijen, M. A.; Andriessen, R.; Kessels, W. M. M.; Creatore, M. Atomic Layer Deposition for Perovskite Solar Cells: Research Status, Opportunities and Challenges. *Sustain. Energy Fuels* **2017**, *1*, 30−55.
(230) Seo, S.; Jeong, S.; Park, H.; Shin, H.; Park, N.-G. Atomic Layer Deposition for Efficient and Stable Perovskite Solar Cells. *Chem. Commun.* **2019**, *55*, 2403−2416.
(231) Toma, F. M.; Cooper, J. K.; Kunzelmann, V.; McDowell, M. T.; Yu, J.; Larson, D. M.; Borys, N. J.; Abelyan, C.; Beeman, J. W.; Yu, K. M.; Yang, J.; Chen, L.; Shaner, M. R.; Spurgeon, J.; Houle, F. A.; Persson, K. A.; Sharp, I. D. Mechanistic Insights into Chemical and Photochemical Transformations of Bismuth Vanadate Photoanodes. *Nat. Commun.* **2016**, *7*, 12012.
(232) Nellist, M. R.; Qiu, J.; Laskowski, F. A. L.; Toma, F. M.; Boettcher, S. W. Potential-Sensing Electrochemical AFM Shows CoPi as a Hole Collector and Oxygen Evolution Catalyst on $BiVO_4$ Water-Splitting Photoanodes. *ACS Energy Lett.* **2018**, *3*, 2286−2291.
(233) Nellist, M. R.; Laskowski, F. A. L.; Qiu, J.; Hajibabaei, H.; Sivula, K.; Hamann, T. W.; Boettcher, S. W. Potential-Sensing Electrochemical Atomic Force Microscopy for in Operando Analysis of Water-Splitting Catalysts and Interfaces. *Nat. Energy* **2018**, *3*, 46−52.
(234) Yu, W.; Fu, H. J.; Mueller, T.; Brunschwig, B. S.; Lewis, N. S. Atomic Force Microscopy: Emerging Illuminated and Operando Techniques for Solar Fuel Research. *J. Chem. Phys.* **2020**, *153*, 020902.
(235) Samu, G. F.; Scheidt, R. A.; Balog, Á.; Janáky, C.; Kamat, P. V. Tuning the Excited-State Dynamics of CuI Films with Electrochemical Bias. *ACS Energy Lett.* **2019**, *4*, 702−708.
(236) Kühn, S.; Dumergue, M.; Kahaly, S.; Mondal, S.; Füle, M.; Csizmadia, T.; Farkas, B.; Major, B.; Várallyay, Z.; Cormier, E.; Kalashnikov, M.; Calegari, F.; Devetta, M.; Frassetto, F.; Månsson, E.; Poletto, L.; Stagira, S.; Vozzi, C.; Nisoli, M.; Rudawski, P.; Maclot, S.; Campi, F.; Wikmark, H.; Arnold, C. L.; Heyl, C. M.; Johnsson, P.; L'Huillier, A.; Lopez-Martens, R.; Haessler, S.; Bocoum, M.; Boehle, F.; Vernier, A.; Iaquaniello, G.; Skantzakis, E.; Papadakis, N.; Kalpouzos, C.; Tzallas, P.; Lépine, F.; Charalambidis, D.; Varjú, K.; Osvay, K.; Sansone, G. The ELI-ALPS Facility: The next Generation of Attosecond Sources. *J. Phys. B: At., Mol. Opt. Phys.* **2017**, *50*, 132002.
(237) Janáky, C.; Hursán, D.; Endrődi, B.; Chanmanee, W.; Roy, D.; Liu, D.; de Tacconi, N. R.; Dennis, B. H.; Rajeshwar, K. Electro- and Photoreduction of Carbon Dioxide: The Twain Shall Meet at Copper Oxide/Copper Interfaces. *ACS Energy Lett.* **2016**, *1*, 332−338.
(238) Bhosale, S. S.; Kharade, A. K.; Jokar, E.; Fathi, A.; Chang, S.-M.; Diau, E. W-G. Mechanism of Photocatalytic CO_2 Reduction by Bismuth-Based Perovskite Nanocrystals at the Gas-Solid Interface. *J. Am. Chem. Soc.* **2019**, *141*, 20434−20442.
(239) Sheng, J.; He, Y.; Li, J.; Yuan, C.; Huang, H.; Wang, S.; Sun, Y.; Wang, Z.; Dong, F. Identification of Halogen-Associated Active Sites on Bismuth-Based Perovskite Quantum Dots for Efficient and Selective CO_2-to-CO Photoreduction. *ACS Nano* **2020**, *14*, 13103−13114.

https://dx.doi.org/10.1021/jacs.0c10348
J. Am. Chem. Soc. 2020, 142, 21595−21614